ESO Document Nr. E-TRE-UVA-222-0101
Issue 1.0 - 28 September 2007

FACULTAD DE CIENCIAS
DEPARTAMENTO DE FÍSICA Y ASTRONOMÍA
DEPARTAMENTO DE METEOROLOGÍA
DEPARTAMENTO DE ESTADÍSTICA

Analysis of local meteorological conditions in Macón using the MM5 modeling system

September 28, 2007

Omar Cuevas, Michel Curé, Carlos Alvarez

Departament of Physics and Astronomy, Valparaíso University

Arlette Chacón

Departament of Meteorology, Valparaíso University

Alejandra Christen

Departament of Statistics, Valparaíso University

Universidad de Valparaíso

Contents

Chapter 1

Introduction

The Macón zone (24°S, 66°W) in the northeast of Argentina, is an area pre-selected for the construction of the ELT (Extremely Large Telescope), which the ESO[1] is in charge of. Preliminary analysis has described this sector as one of the optimal zones of our plant for this activity. These studies were done within the framework of selecting a site for ESO astronomic observation [Sarazin et al., 2000]. Due to interest in this zone, *in situ* measuring campaigns have been conducted of variables which condition the place, among those meteorological and turbulence information is considered important for astronomic observation. This information will be analyzed relating seeing (turbulence) cases to local and synoptic meteorology, in order to identify the flow pattern in an area that is considered to be orographically complex.

In order to study the meteorology of this place the MM5 modeling system will be used, whose characteristics make it possible to do small scale analysis ($\sim$1 km), and it integrates the most modern and realistic parameterization schemes of a variety of atmospheric physical processes, which are appropriate to the conditions present in Macón.

In this report, climatic and orthographic descriptions were done first and are described in chapter 2. Chapter 3 shows the data used in this study. The configuration of the MM5 modeling systems for Macón is described in chapter 4. A synoptic analysis and classification of flow patterns of the Macón zone were conducted and are described in chapter 5. Chapter 6 shows the MM5 model validation that was performed using real data registered for the meteorological station in Macón. Next, in chapter 7 trajectories of different spatial scales were analyzed in order to determine the origin of the air flow that reaches Macón. In the following chapter (8), a statistical analysis was done of the seeing variable for Macón, and then a study of seeing was conducted where local meteorological variables were related to turbulence indices, such as the TKE and the Richardson number (Ri). Chapter 10 discussed the most relevant conclusions of this study.

1.1 Motivation

In Macón turbulence data was collected and saved over a total of 158 nights using the MASS (Multi Aperture Scintillation Sensor) and DIMM (Differential Image Motion Monitors) instruments. This information forms part of the preliminary studies conducted by the ESO when searching for a site to

[1] European Southern Observatory

build the ELT. To analysis this data as well as the numerical simulations using the MM5 model and thus understand the meteorological conditions in Macón are the main motivations for this study.

1.1.1 Main objetive

To analyze the local meteorology of Macón using the MM5 modeling system, along with data obtained in different campaigns.

1.1.2 Specific objectives

1. Implement the MM5 model for the Macón zone.
2. Statistically analyze the measured turbulence data (Cn^2) and seeing through time and identify relevant episodes as case selections.
3. Do simulations for the cases selected.
4. Analyze the synoptic conditions of the simulations carried out.
5. Analyze and compare the turbulence indices TKE and the Richardson number (Ri) and other meteorological variables with turbulence data (Cn^2) and seeing.

Chapter 2

Climatology and orography of Macón

2.1 Climatology of Macón

The majority of the literature reviewed (Rutllant, 1982; Ulriksen, 2001a) expressed that the most important factors that control the atmospheric weather and conditions the climate throughout continental Chile are the Subtropical Anticyclone of the South Pacific, the cold oceanic circulation of Humboldt, the winds from the West zone where the frontal systems and cut of low flow travel, and further South are the low pressure zones which surround the Antarctic, known as circumpolar trough. Furthermore, in the North of Chile, in the summertime the monzonic circulation developed on the East side of the Andes Cordillera generates precipitation in the altiplane.

For the Macón zone, located in the middle of the Andes Cordillera in Argentine territory, one must take special consideration of the predominance of warm anticyclone of the Subtropical Anticyclone of the Pacific South (PA), the zone of the West Winds (WW) that constantly advect masses of cold air, inducing frequently dominated as high trough (HT) and migratory cold anticyclones (CA). Furthermore, it is important to consider the altitudes effects on jet streams both subtropical and polar (JS), and during the summertime periods, the monozonic circulation of the altiplane and Altiplane Winter (AW) have an influence.

Other circulations to consider are more closely related to South American climatology where the Continental Warm Low (WL) is considered the most important, which is developed at low levels like the warm and humid tongue in the central Brazil and that moves approximately from North to South for the center of the continent, with a maximum intensity in the summertime period. On the other side, the local climate of Macón corresponds to the cold desert of the mountain whose most relevant characteristic is very dry air and where the rhythm of the temperatures is regulated by the altitude. The type of ground is characterized by the dominance of more drastic conditions of dryness.(Alvarez, 2004).

There is big thermal amplitude in the levels closest to the surface in the desert, with strong contrast of temperature extreme between day and night. Additionally, in the valleys and couffin appear valley-mountain breezes. In atmospheric movements on a small scale, local effects predominate such as the interaction with the surface, relief and obstacles.

In order to analyze the Macón zone, it is necessary to identify the most influential synoptic climatology, which entails looking for circulation patrons in South America at synoptic scale. Following are the climatologically composites of the most relevant variables.

2.1.1 Temperature

In analyzing the climatologically variable of temperature, it can be observed that at low levels (925 hPa), a warming elongation from the center of Brazil toward the South is clearly delineated, describing the circulation of the WL. In the sector the Pacific Ocean it can be observed that the incursion of cold air reflecting the influence of the ocean current of Humboldt, helping the climatic stability of the North of Chile (figure 2.1a). It can be assumed that the temperature contributions that arrived at Macón, from low levels, depends on the behavior of the WL and PA.

In the 500 hPa, it can be observed that climatically over Macón soft incursions of HT are elongated, where in the trough sector enters slightly cold air and in the ridge enters warm air with a climatologically isotherm of -8 degrees Celsius (figure 2.1 b). For the 250 hPa there is a very established margin zone with an isothermal mean of -43 degrees Celsius (figure 2.1 c).

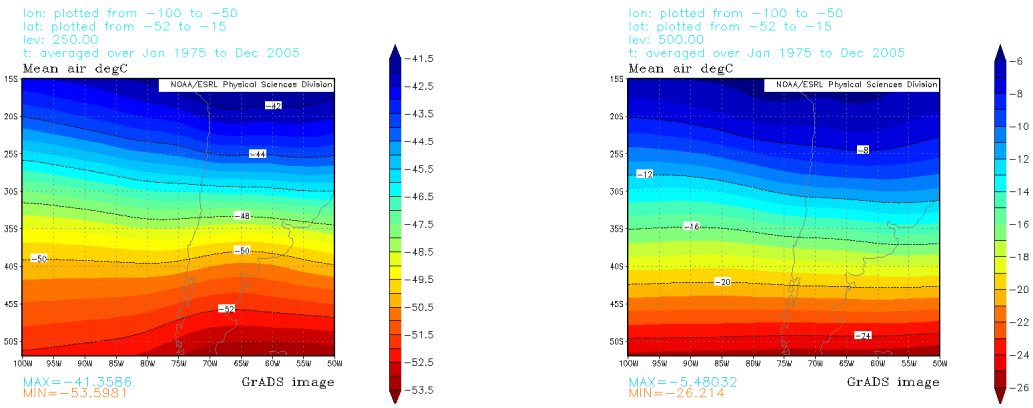

a) b)

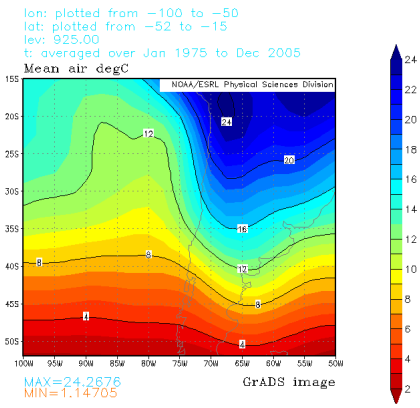

c)

Figure 2.1: Temperature climatology (a, b, c) in 950, 500 and 250 hPa. Reanalysis images taken (NCEP).

2.1.2 Geopotential Height

For the level of the 925hPa, above the Pacific Ocean, the predominance subtropical anticyclonic semipermanent in the zone can be observed (AP), which is related to the elongation of low pressure values of the coastal low (CL), patterns that circulate from north to south along the coast of Chile. In addition, in the southern zone the WW are shown, patterns where the frontal systems flow travel, and where the entrance of these frontal system toward the north barely entering to continent. Also, the prolongation above the continent of the WL can be observed (Figure 2.2a). On the 500 hPa is an approximate average of 5850 mgp (geopotential meters) for Macón with incursions of HT (Figure 2.2b). On the 250hPa zonality is observed (Figure 2.2c).

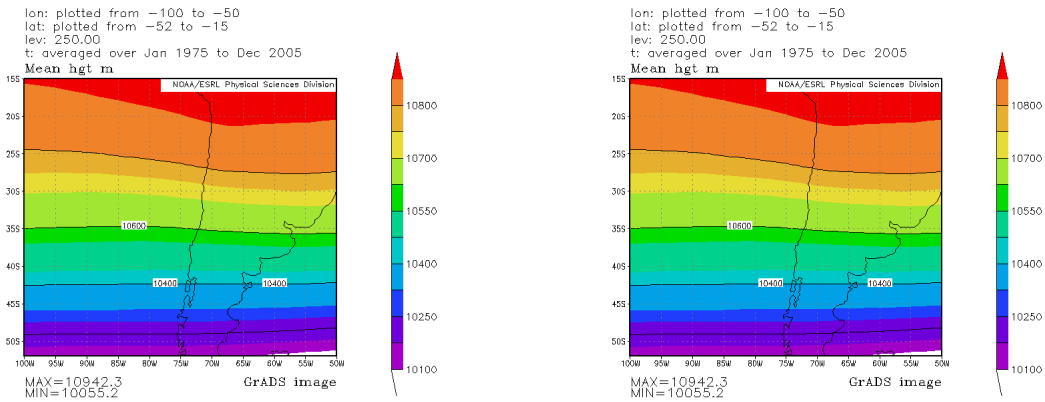

a) b)

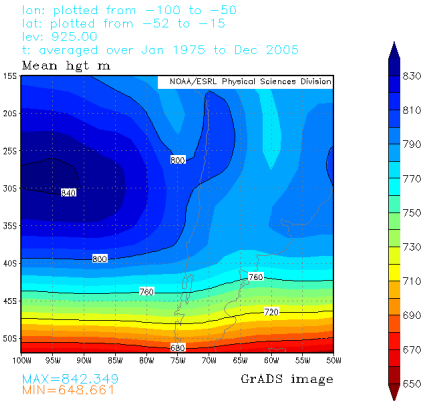

c)

Figure 2.2: Climatology (a, b, c) and anomaly (d, e, f) of geopotential height at 950, 500 and 250 hPa. Images taken from reanalysis (NCEP).

2.1.3 Relative Humidity

Climatically speaking, it can be observed in the zone of Macón is especially dry with very low relative humidity in the 925 hPa (Figure 2.3a). Analyzing the level of 500 hPa, it shows a minimum relative humidity from the Northwest associated mainly with PA, whose influence is noticeable (Figure 2.3b). For the level of the 300 hPa the same pattern of the 500 hPa can be observed, with the difference being that it is slightly moved North (Figure 2.3c).

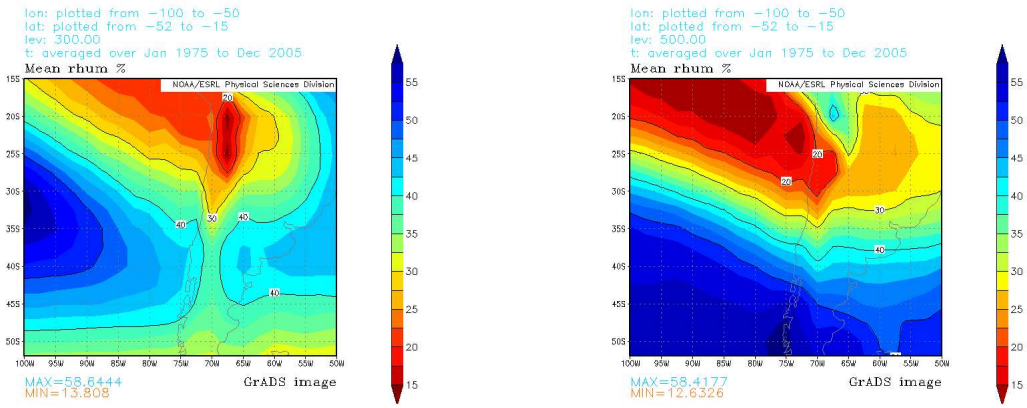

a) b)

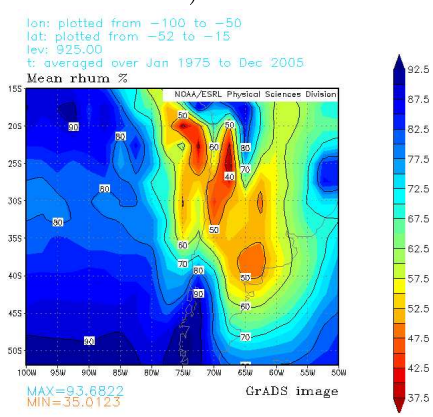

c)

Figure 2.3: Climatology (a, b, c) of relative humidity 950, 500, and 300 hPa.. Images taken from reanalysis (NCEP).

2.1.4 Omega (dp / dz) vertical air movement

Here the pattern of the 925 hPa shows us a zone with slightly negative values, implying elevation of air by orographic character by way of air flow from the East, along with the monozonic circulation of AW of the summer (Figure 2.4a), while in the 500 hPa there exist a sector in a great portion of the cordillera,

including Macón, with maintained elevations, which are associaded again with the orographic effects and the contributions of air from lower levels of the WL and the AW, also the PA with its maintained air descents (Figure 2.4b). The level of the 250 hPa continue to show the PA although with greater intensity, which guarantees general circulation model of the atmosphere yielding climatically speaking a sector of air descent over the Pacific Ocean, commonly known as the limit between the circulations of the cells of Ferrel and Hadley (Holton, 1990), while for Macón there are slight elevations (Figure 2.4c).

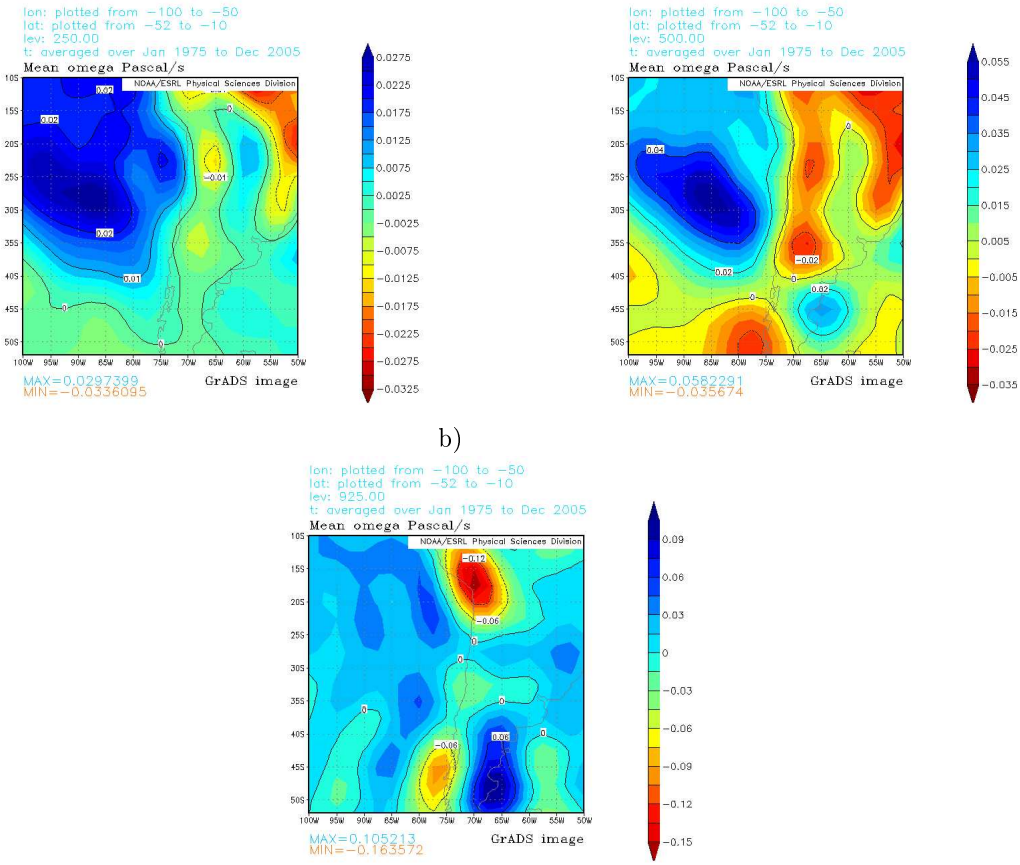

a) b)

c)

Figure 2.4: Climatology (a, b, c) of Omega (dp/dz) at 950, 500 y 300 hPa. Images taken from reanalysis (NCEP).

2.1.5 Wind Vector

For the 925 hPa a center of cyclonic circulation exists climatically speaking in the Macón zone, where air comes from the West, product of the PA, and from the East due to the circulation of the WT (Figure 2.5a). In the 500 hPa the effect of the HT is observed as a change in the wind intensity and

direction, the climatological value of the module of the wind over Macón approximates the 10 m/s (Figure 2.5b). In the level of the 250 hPa a semipermanent JS can be identified that is elongated from the West – Northwest to the East – Southeast associated to the birthing zone of the frontal systems, which are also called frontalgenetic zones, whose nucleus is approximately between Uruguay and the South of Brazil, whose effects spread to the Macón zone (Figure 2.5c).

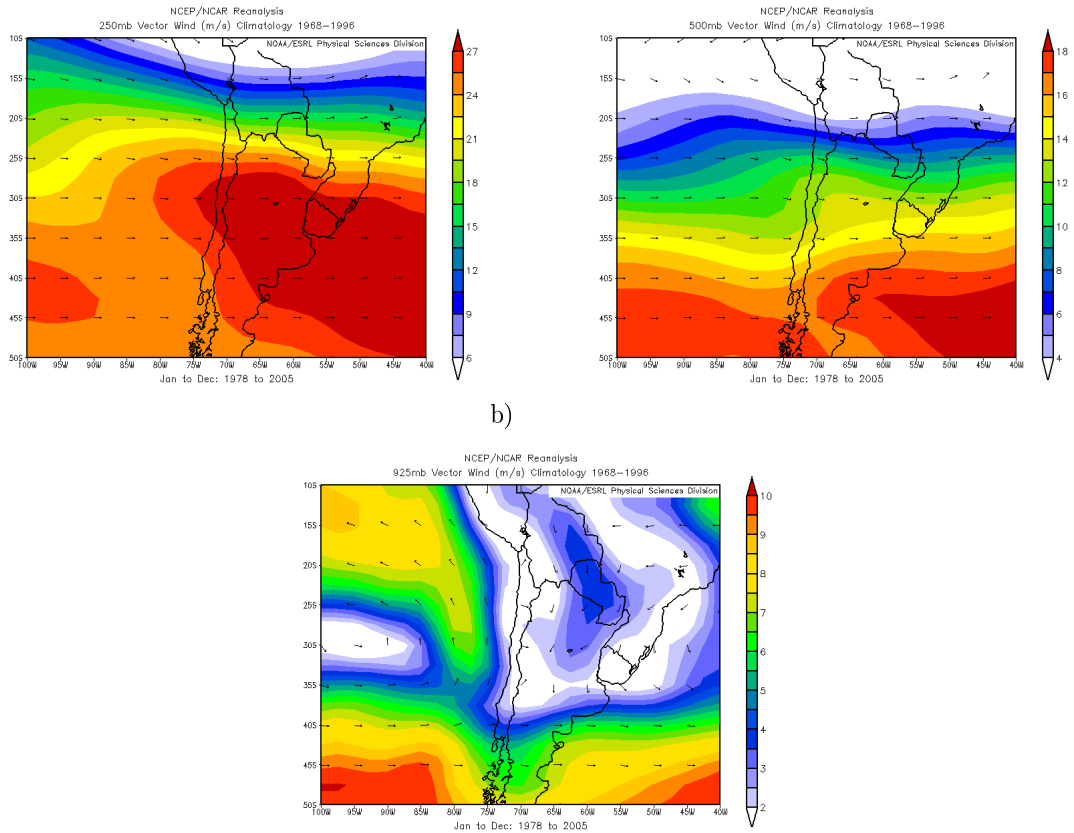

a) b) c)

Figure 2.5: Wind climatology in 950, 500 y 250 hPa. Images taken from reanalysis (NCEP).

2.1.6 General Description

With the local characteristics of the Macón zone, we can highlight that the radiative balance and therefore the temperature, are fundamental in the climatic modulation. This means that the climate has a radiative character, which means that within a normal year there are not great variations associated with advections of air form the other zones.

Despite this, in the analysis of the synoptic climatology you can identify the different circulations that dominate above the South American continent, the most influential over Macón, of semipermanent

character are: the PA associated with the subtropical anticyclone of the Pacific, the circulation of low levels of the

WL, and the monozonic circulation of AW. Now, in synoptic patterns that move, we find the HT which occur often, JS and CA that have a lesser presence. In addition, there exist very few incursions of frontal systems and segregated lows during the year.

In function of local factor and of synoptic climatology, we can sum up by saying that the Macón zone has many thermal variables, which bring consequences that the type of ground conditions a local, daily (day and night). In addition, if we add up the patterns of circulation that move, the curve of normal climatological variables of the Macón zone, suffers small changes throughout the year, mainly by HT and JS, patterns that present interseasonal periods. The variable relative humidity is the most regular of all. Its extension temporary and special including vertically, since it is an extremely dry zone.

It is important to emphasize the semipermanent patterns also suffer changes in function of more extensive circulations both temporarily and special, just like the Niño and the Southern Oscilation (ENSO) or the Antarctic Oceanic Circulation (SSA). These patterns present periods within decades, which is out of the scope of this study.

It is important to point out that the semipermanent patterns also suffer changes in function of more extensive circulations both temporarily and special, just like el Niño and the Southern Oscilation (ENSO) or the Antarctic Oceanic Circulation (SSA). These patterns present periods within decades, which is out of the scope of this study.

2.2 Orography

Macón is located to the northwest of Argentina, almost at the border with Chile on the west side of the Andes Cordillera. In Figure 2.6 the mountain chain of the Macón zone can be seen, which extends west to the salt lake Arizaro. In Macón summits are found until 5,000 m.a.s.l. and meteorological station is at 4,6000 m.a.s.l. Toward the southwest is Tolar, a place where turbulence measurements were taken by the MASS instrument, which serve as a bases for this study. This station is found at a height of 3,500 m.a.s.l. with approximate difference of 1 km with respect to Macón.

Figure 2.6 shows the comparison between two sources of data that describe the zone, to the left a digital picture from Google Earth is shown, while on the right a digital picture of the zone used by the MM5 model. This comparison reflects the detail that the MM5 model provides, because of the influence of the complex orograph and local circulation is captured and it is possible to establish better performance of previous analyses.

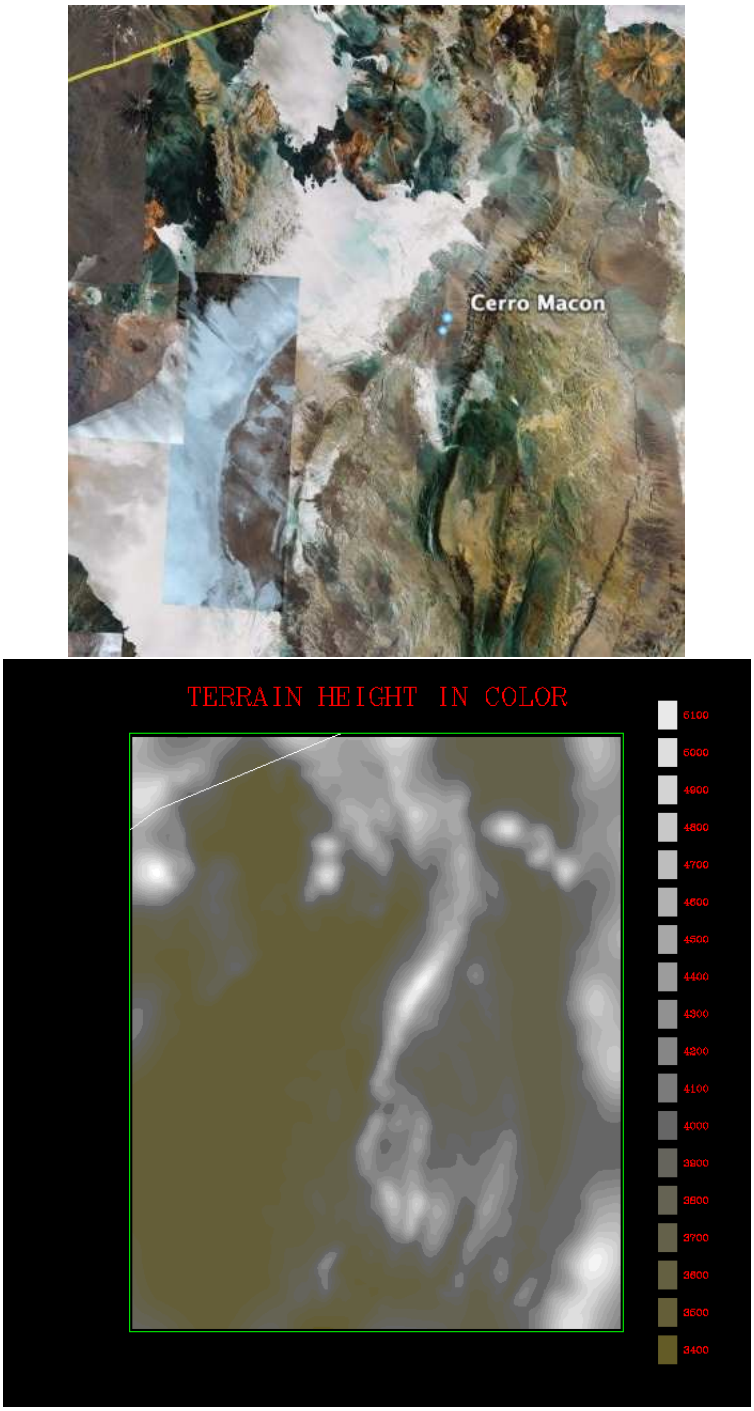

Figure 2.6: Orograph of the zone studies, above an digital image by Google Earth, below domain 4 utilized by the MM5 model.

Chapter 3

Data

For this study, tree main sources of data corresponding to meteorological information of global models (GFS model and mesoescale model MM5), data of data of atmospheric turbulence and seeing taken by ESO in the Macón zone are used. Meteorological data of an automatic station implemented in the zone and infrared satelital images by GOES-12.

3.1 GFS global model data

The NCEP[1] has developed a numerical model of the planetary atmosphere, with the purpose being to support the work done in forecasting and research in meteorology. This model has become a fundamental tool in the area of meteorology world wide. In addition, this information has served as a basis for the development of more sophisticated tools in the area of atmospheric sciences.

The global numerical model of the NCEP is currently the GFS[2], which has be programmed to model the earth's atmosphere in horizontal resolution grids of 1.25 degree and a vertical resolution grid of 12 pressure levels starting from 1000 hPa to 70 hPa. Temporarily this data reaches 120 hours of forecasting. The model is run four times a day every six hours (00Z, 06Z, 12Z, 18Z). The runs are started based on the observations registered for the majority of the reports that exist officially around the world at earth, sea and air meteorological stations.

For this study the data available from the ftp site of the NCEP corresponding to the octal half of south America situated between 0^oS to 90^oS latitude and 120^oW to 30^oW longitude was used. The Universidad de Valparaíso has a database for this model starting in June 2004 and going through August 2006.

The GFS data will serve as boundary and initial conditions for the high resolution MM5 modeling over the Macón area (Argentina, 24^oS, 66^oW). Due to its closest geographically location, these calculations can be applied to Paranal (Chile, 24.6^o, 70.5^oW) and ALMA (Chile, Chajnantor, Atacama Desert) as well.

In the appendix, the script which is currently used to download this information automatically and daily is shown.

[1] National Center for Environmental Prediction. *www.ncep.noaa.gov*
[2] Global Forecast System. *ftpprd.ncep.noaa.gov*

3.2 Meteorological data

In Macón one finds a weather station installed near the summit located al 4600 m.a.s.l. and registers the following meteorological variables: temperature at 2 metres, intensity and wing direction at 10 metres and relative humidity. These records will serve to be compared with the results of the model MM5 applied to the zone. In addition we used infrared satelites images of GOES-12 for 00z and 09z in the period of the study.

3.3 Turbulence data (MASS-DIMM)

In Macón, vertical atmospheric turbulence data has been registered, using the MASS instrument (Multi Aperture Scintillation Sensor). This instrument registers turbulence (C_n^2) at six different height levels (0.5, 1, 2, 4, 8, 16 KM) as they related to time. These registries allows also to obtain the value of seeing, variable analized in later chapters.

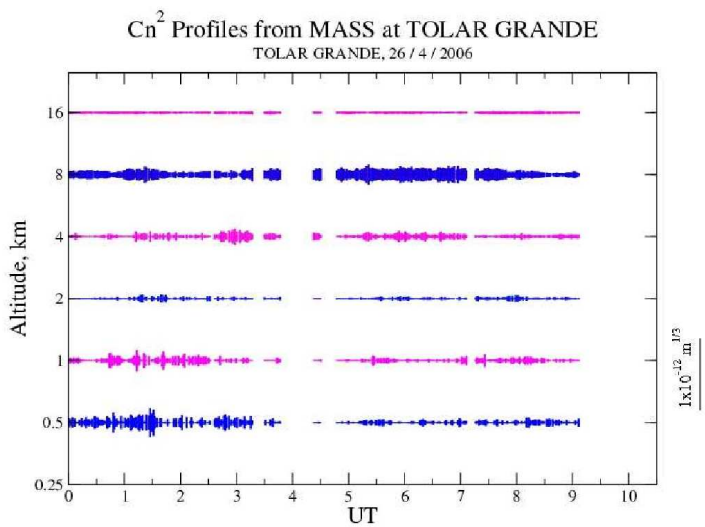

Figure 3.1: A nigth of turbulence profile by MASS (26/04/06).

ESO in Macon has made 6 campaigns of measurament of turbulence and seeing with MASS instrument, during the period between March 10, 2005 and April 28, 2006 whith a total of 158 night of data of atmospheric turbulence.

Also in Macon, were made campaigns of measurement with DIMM (Diferencial Image Motion Monitors) with a total of 30 nights of registration od data, between May 30, 2005 and April 28, 2006.

The data used in this study correspond to the registered by MASS instrument in the zone of Tolar (24° 35'S, 67° 24'W) corresponding to 126 nights of record between the months of March to December of 2005.

The following table summarizes the number of records of data available and used in this study.

Turbulence (Cn2)	Global Model (GFS)	Weather station
126 nights	118 days	113 days

Table 3.1: Nigths sample

Chapter 4

Description of the MM5 model system

The MM5 modeling system, currently in its fifth generation, was developed by Pennsylvania State University (PSU) and the NCAR[1]. This model is used in several universities and institutions around the world because of its high definition in mesoscale atmospheric systems. The model solves numerically the equations of the atmosphere, which are equations of momentum, mass, and energy conservation.

Satisfactory results have been found in the southern hemisphere [see eg., Garreaud, 1999], thus this model can be applied it in the sector under study in this research.

Important aspects of the model are [MM5 home page[2]]:

1. Multiple nesting capacity with "two-way" interaction between domains. This facilitates the study of atmospheric phenomena using different space scales and the design at very high resolutions forecast.

2. Formulation of a non-hydrostatic dynamic, which alows the model to be used efficiently to represent phenomena with small spatial dimensions, that is, of very few kilometers.

3. Adaptation for multiple plataforms and in computers of shared or distributed memory.

4. Automatic ingest of data from different meteorological analisys and observation sources, including the capacity to assimilate data in 4-dimensions.

5. Variational assimilation of conventional data and satellites during forecasting.

6. Incorporation of the most modern and realistic parameterization schemes of physical processes related to atmospheric radiation, clouds and precipitation microphysics, convection by cumulus, turbulence, energy flow and momentum on land surface.

The MM5 suite has pre and post process programs, in the following section the pre-process modules are described briefly. They are fundamental to the functioning of the suite and are the same ones that are implemented in developing this research.

[1] National Center for Atmospheric Research
[2] www.mmm.ucar.edu/mm5

4.1 TERRAIN module

This module belongs to the MM5 suite, and it is in charge of configuring the domains for the simulations that follow. The main characteristics of this module are the land configuration with different horizontal resolutions and the formation of grids for the posterior process. It is also here where the type of land elevation, ground type and use, vegetation, and other types are selected. It has resolutions that go has high as 900 m for land information. For us what is essential is the selection of the type of land surface use (LSM[3]) in order to integrate the variable TKE (Turbulent Kinetic Energy) which is important for posterior seeing analysis.

Four domains are configured for this study (Fig. 3.1):

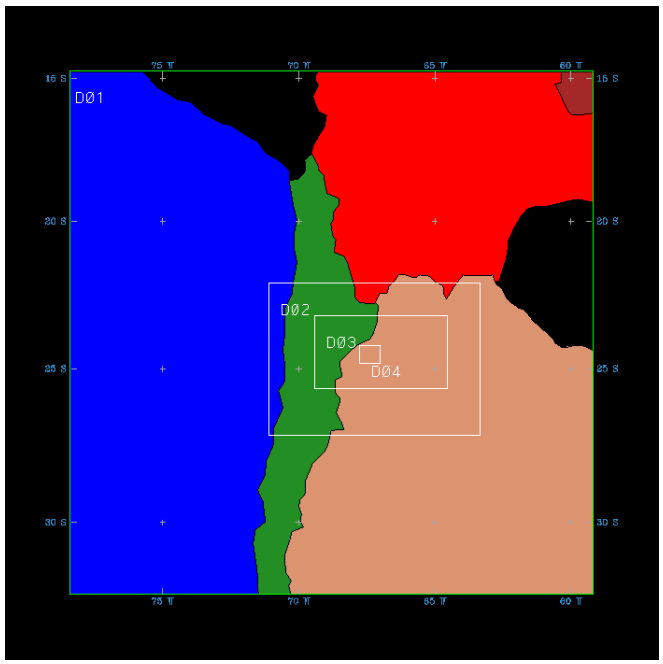

Figure 4.1: Domain maked whith TERRAIN for simulations of the MM5 model

1. D1: 80x80 grid points and 27 km of horizontal resolution. Use of global land and ground to 19 km. (Mother Domain)
2. D2: 70x97 grid points and 9 km of horizontal resolution. Use of global land and ground to 9 km.
3. D3: 100x181 grid points and 3 km of horizontal resolution. Use of global land and ground to 4 km.
4. D4: 73x85 grid points and 1 km of horizontal resolution. Use of global land and ground to 1 km.

[3] Land-Surface Model

4.2 REGRID module

This module belongs to the pre-procedural entrance data used for simulation in MM5. It is divided in two submodules which fulfill different functions, assigned to process the type of entrance data with the different meteorological information it possesses.

4.2.1 Pregrid

This module reads the data in GRIB format (format of available data from GFS and ECMWF). In our case it is configured for the GFS and ECMWF input data.

The data created for this module are of type:

- FILE: (date) = meteorological data corresponding to height levels.
- SST_FILE: (date) = surface sea temperature data.

4.2.2 Regridder

This module is in charge of recalculating the GRIB data to the grids generated with TERRAIN. The exits of this module are an example of type:

- REGRID_DOMAIN1 (for domain 1)

This data has surface and pressure level (3d) intergrated information with a time frequency of 6 hours in this case.

4.3 INTERPF module

This module is in charge of generating the initial conditions in order to start the numerical simulations with MM5, in our case starting with the GFS global model. In this model the "sigma" (σ) levels for height (Fig 3.2) are added replacing the pressure coordinates for the GFS data heights . The sigma levels have the advantage of following the orography and are related to the pressure at different height levels by the following equation:

$$\sigma = (p - p_t)/(p_s - p_t)$$

Where p is the actual pressure, p_t constant pressure of the top reference, p_s is the surface reference pressure.

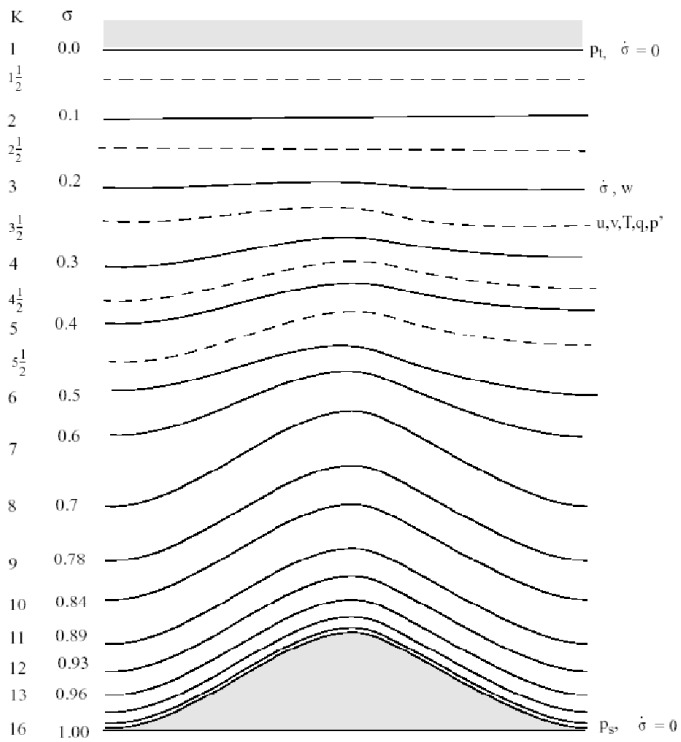

Figure 4.2: Sigma levels integrated by MM5 model

In our case 30 sigma levels were used. They are described as follows.

1.00, 0.99, 0.98, 0.96, 0.93, 0.89, 0.87,
0.85, 0.80, 0.75, 0.70, 0.65, 0.60, 0.57,
0.55, 0.50, 0.45, 0.40, 0.35, 0.32, 0.30, 0.27,
0.25, 0.23, 0.20, 0.17, 0.15, 0.10, 0.07, 0.05, 0.00

Subsequently, this MM5 module reads the files processed in regridder and creates the following exit files:

- MMINPUT_DOMAIN
- BDYOUT_DOMAIN
- LOWBDY_DOMAIN

These files are those needed to start a simulations with the MM5 model.

4.4 MM5

The model for this study has been configured using parameterizations that adapt better to the orographic conditions of the zone and also have a higher horizontal resolution. (∼1 km).

1. Schultz microphysics: A highly efficient and simplified scheme (based on Schultz 1995 with some further changes), designed for running fast and being easy to tune for real-time forecast system. It contains ice and graupel/hil processes. [Internet reference 1].

2. Kain-Fritsch scheme cumulus: Similar to Fritsch-Chappell, but using a sophisticated cloud-mixing scheme to determine antrainment/detrainment, and removing all available bouyant energy in the relaxation time. This scheme predicts both updraft and downdraft properties and also detrains clouds and precipitation. Shear effects on precipitation efficiency are also considered.[Kain and Fritsch, 1993].

3. Eta Planetary boundary layer parameterization: This is the Mellor-Yamada scheme as used in the Eta model, Janjic (1990, MWR) and Janjic (1994, MWR). It predicts TKE and has local vertical mixing. The scheme calls the SLAB routine or the LSM for surface temperature and has to use ISOLI=1 or 2 (not 0) because of its long time step. Its cost is between the MRFPBL and HIRPBL schemes. Before SLAB or the LSM the scheme calculates exchage coefficients using similarity theory, and after SLAB/LSM it calculates vertical fluxes with an implicit diffusion scheme. [Internet reference 1].

4. RRTM[4] longwave scheme: This is combined with the cloud-radiation shortwave scheme when IFRAD=4 is chosen. This longwave scheme is a new highly accurate and efficient method provided by AER INC. (Mlawer et al. 1997). It is the RRTM and uses a correlated-K model to represent the effects of the detailed absoption apectrum taking into account water vapor, carbon dioxide and ozone. It is implemented in MM5 to also interact with the model cloud and precipitation fields in a similar way to IFRAD=2.

5. Five-Layer Soil model: Temperature predicted in 1,2,4,8,16 cm layers (approx.). with fixed substrate below using vertical diffusion equation. Thermal inertia same as force/restore scheme, but vertically resolves diurnal temperature variation allowing for more rapid response of surface temperature.

[4] Rapid Radiative Transfer Model

Chapter 5

Synoptic analisys

In this chapter the synoptic analysis of the period used in this study (Chapter 3) is described starting with the synoptic classification done using the results of the MM5 model and the support of infrared satellite images GOES -12.

5.1 Synoptic classification

The classification is based on the characteristic synoptic episodes that are found in the central – western part of South America, which control the climate of this region and which form part of the Macón zone. Six characteristic synoptic episodes where classified using the results of domain 1 of the simulations done with the MM5.

5.1.1 Anticyclonic Predominance (AP)

The semi-permanent subtropical anticyclone of the Pacific is the great climate regulator characteristic of the west cost of the central and northern part of South America. This anticyclone, having warm characteristics, is present until the boundary of the troposphere (tropopause) and has slow, cloudy descending movements, characteristic of stratus y stratocumulus clouds at low levels. At Macón's latitude, it is one of the great climate regulators present almost year round.

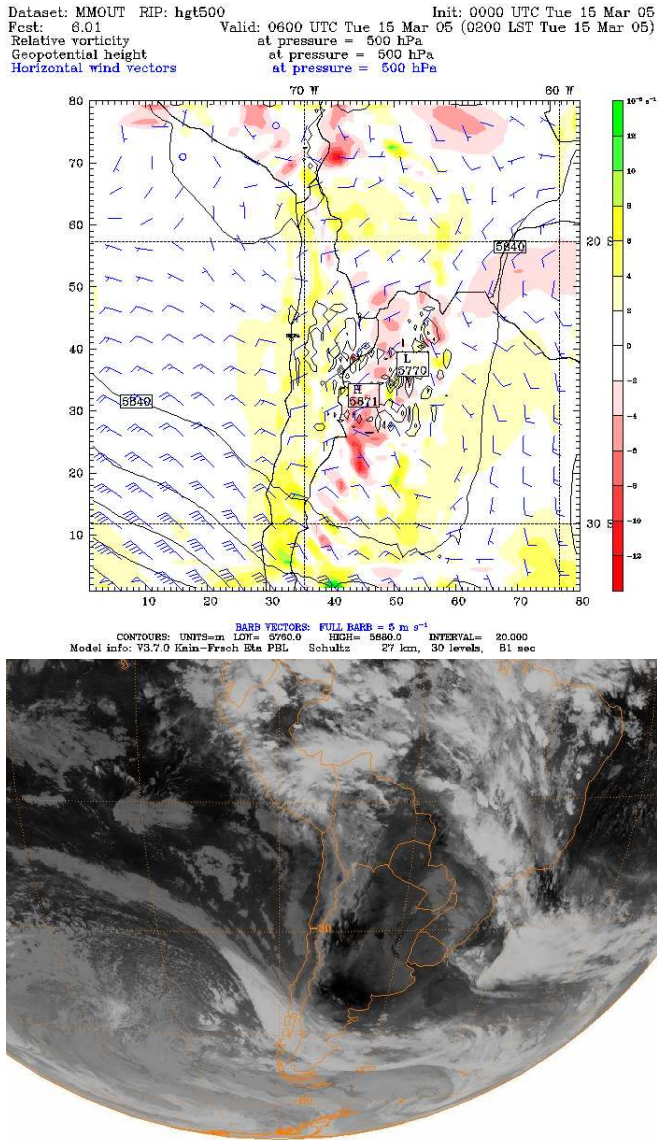

Figure 5.1: AP for the 15/03/05. Above, chart of 500 HPa en domain 1 of the MM5, black lines are the geopotential height, wind is represented in vector form and shaded colors represent relative vorticity. Below, infrared satellite image of GOES - 12. Images representative of the 00Z.

5.1.2 Frontal System (FS)

The frontal systems are formed mainly due to the thermal, humidity, and density differences between two air masses of distinct origins. The fronts that affect Chile are formed in the Pacific Ocean by the collision of masses of dry and cold air having subpolar origins and masses of warm, humid air having

subtropical origins. The frontal systems are the major source of precipitation in the central part of Chile [Garreaud, 1999] and part of the atmospherical perturbation can reach areas like the Macón zone.

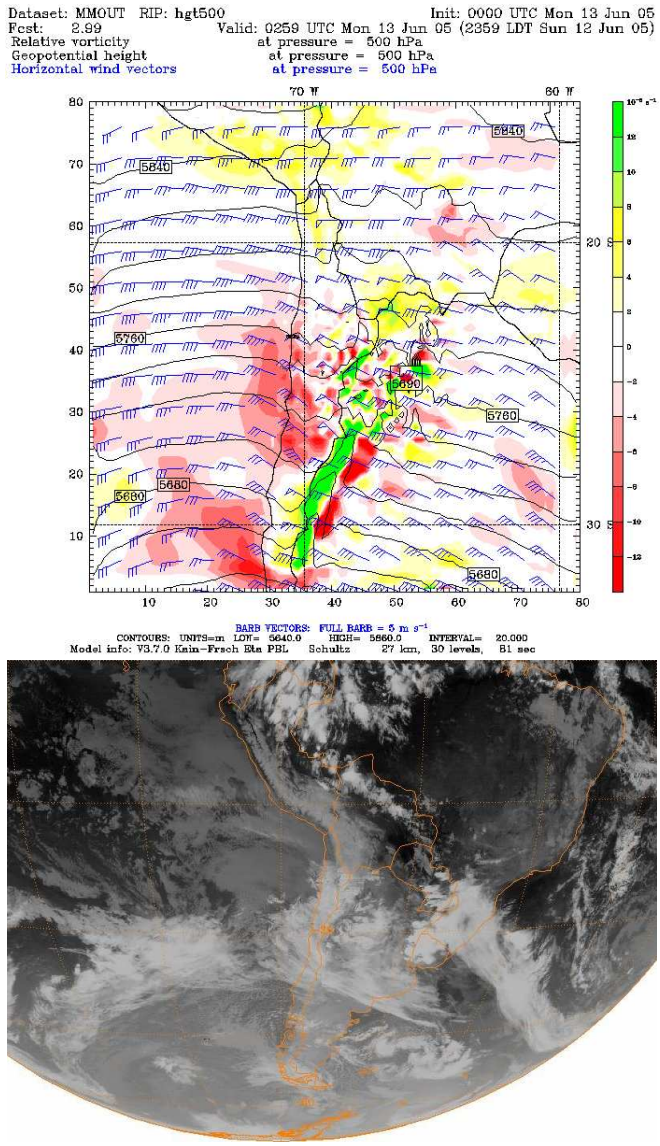

Figure 5.2: FS for the 12/06/05. Above, chart of 500 HPa en domain 1 of the MM5, black lines are the geopotential height, wind is represented in vector form and shaded colors represent relative vorticity. Below, infrared satellite image of GOES - 12. Images representative of the 00Z.

5.1.3 Cut-off Low (CL)

The cold nucleus in cut-off low corresponds to air that is colder than its surroundings, which because of circulation continues turning cylonicly forming trough and fronts in altitude. Such manifestations can be generally be seen in the middle and high atmosphere, where a major source of bad weather is in the cordillera arriving further north than the frontal systems that generally reach the central part of Chile. It is common to see such nucleus in the charts of 500 HPa located 5.500 geopontential meters.

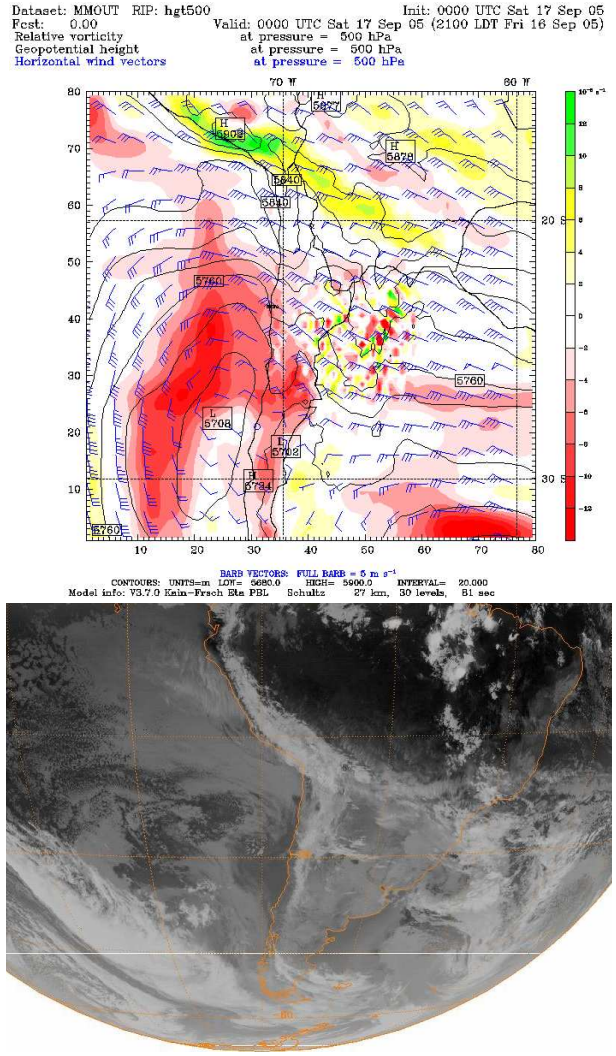

Figure 5.3: CL for 16/09/05. Above, chart of 500 HPa en domain 1 of the MM5, black lines are the geopotential height, wind is represented in vector form and shaded colors represent relative vorticity. Below, infrared satellite image of GOES - 12. Images representative of the 00Z.

5.1.4 Jet Stream (JS)

The jet stream is located almost at the upper boundary layer of the troposphere (tropopause) and JS is generated mainly due to the thermal differences between the air masses that are found at high altitudes. In the southern hemisphere two jet streams can be distinguished: one being subpolar and the other subtropical, both determined by its formation origin. It is known that the maximum speed of wind of the jet stream generate turbulence in its nucleus surrounding (Holton, 1996). The jet stream is present at low and middle latitudes, being observed in the Macón zone.

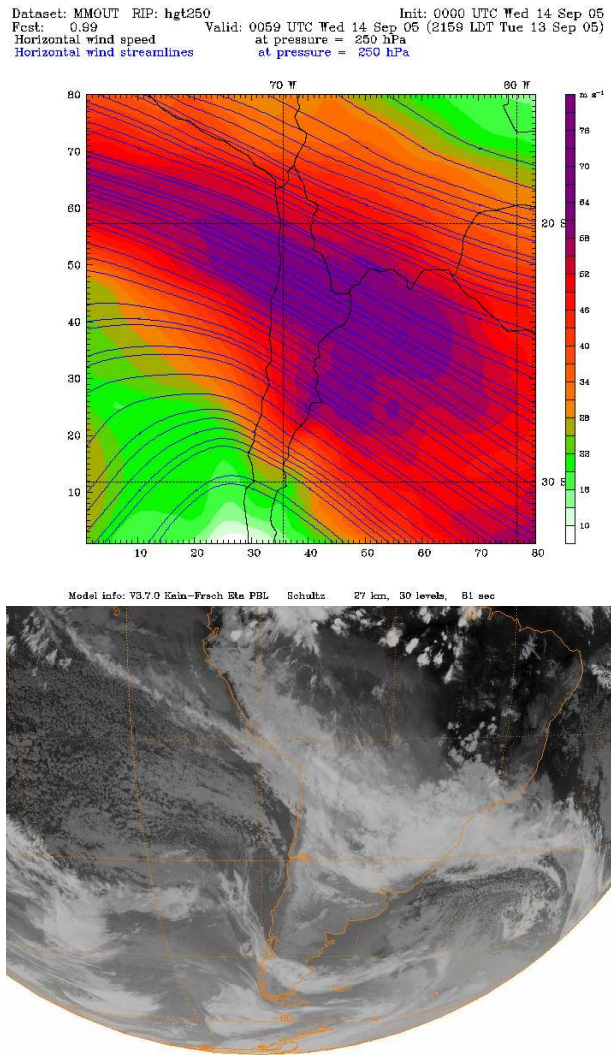

Figure 5.4: JS for the day of 14/09/05. Above is the wind speed maximum in dark colors, the blue lines are the lines of the wind current. Below infrared satellite image of GOES - 12. Images representative of the 00Z.

5.1.5 High Trough (HT)

The troughs are wave prolongations of cyclonic circulation, which can be associated with cut-off low or frontal systems. These waves can be of subsynoptic scales both spatial on temporily (less than 24 hours). These show up in the mid and high troposphere, and are quite common in the cordillera area, and can affect the Macón area. These bring consequently ascending movements and therefore inestability in the front part of the trough and descending movements (stability) in the posterior part of trough. In addition, they can come up during short weather periods (circa one day).

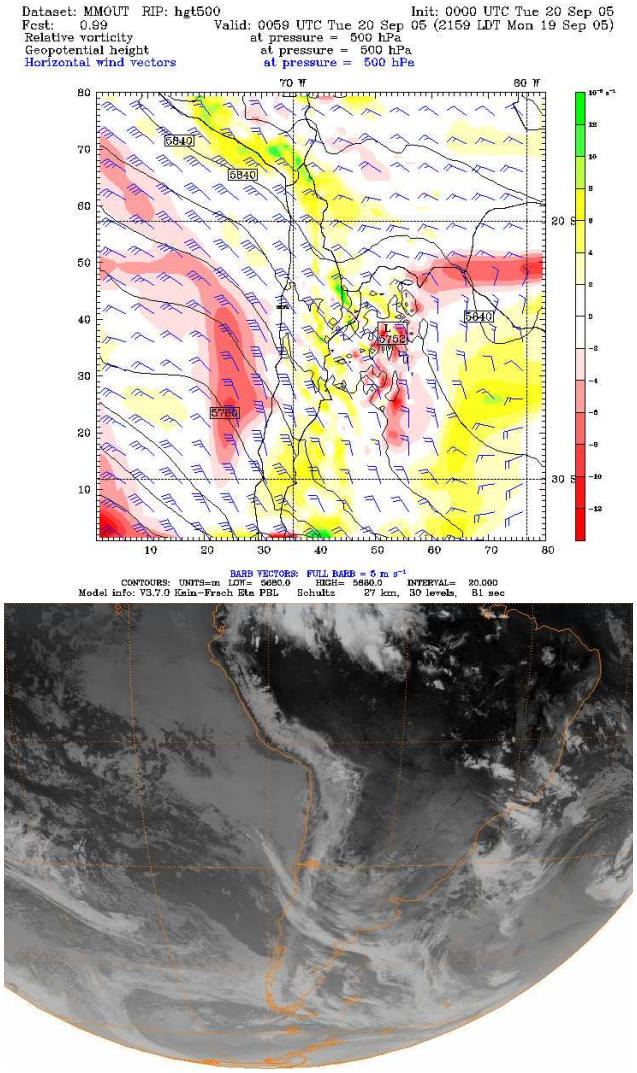

Figure 5.5: HT for the day of 20/09/05. Above, chart of 500 HPa en domain 1 of the MM5, black lines are the geopotential height, wind is represented in vector form and shaded colors represent relative vorticity. Below, infrared satellite image of GOES - 12. Images representative of the 00Z.

5.1.6 Cold Anticyclone (CA)

The CA are cold air masses from high pressures that move behind a cold frontal systems and have cold, dry thermal characteristics and greater density than its surroundings. They migrate traveling across thousands of kilometers and are associated with low temperatures and cloudy stratiform located at low levels close to the ground. Some of them can reach the Macón area.

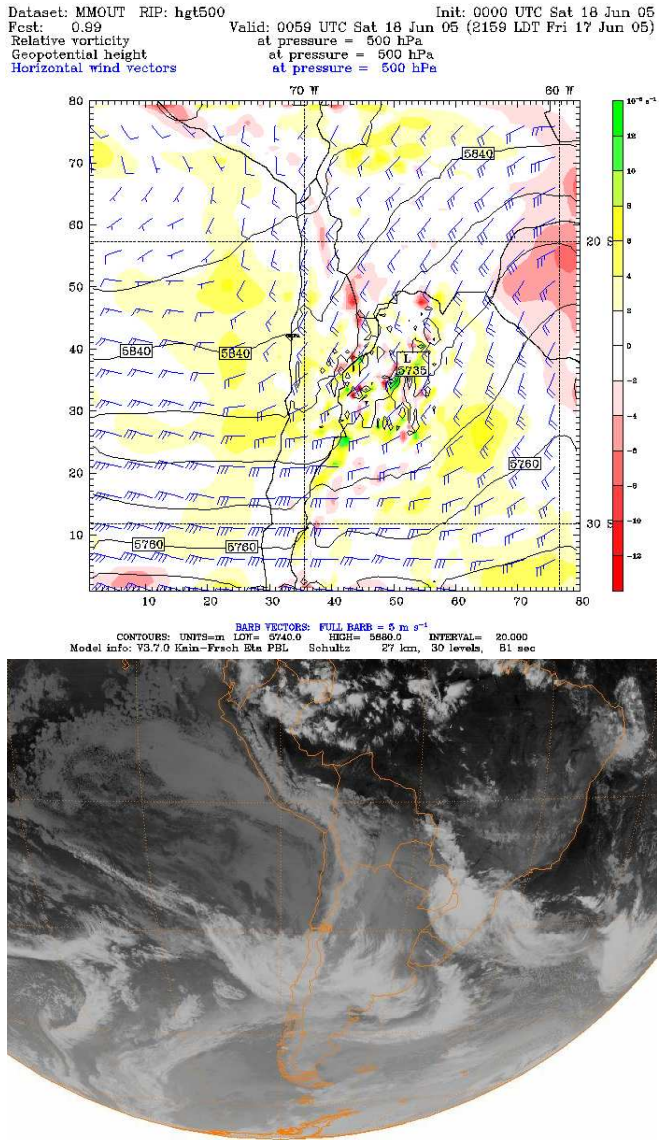

Figure 5.6: CA for the day of 180605. Above, chart of 500 HPa en domain 1 of the MM5, black lines are the geopotential height, wind is represented in vector form and shaded colors represent relative vorticity. Below, infrared satellite image of GOES - 12. Images representative of the 00Z.

5.1.7 Synoptic pattern in Macón

Applying this classification for the 118 cases modeled by MM5 and corresponding to the days for measuring turbulence and seeing for the MASS station in Tolar, what was found was that for most days the anticyclonic predominance was present (AP), followed by high trough (HT), and the jet stream

(JS) as possible atmospheric disturbances. It is important to note that more than one synoptic episode can occur in a night, in some cases even simultaneously which means that they are not exclusive within themselves. This explains, then, why the sum of the number of events might be more than the total number of nigth analyzed. Figure 5.6 shows the distribution of events in the period.

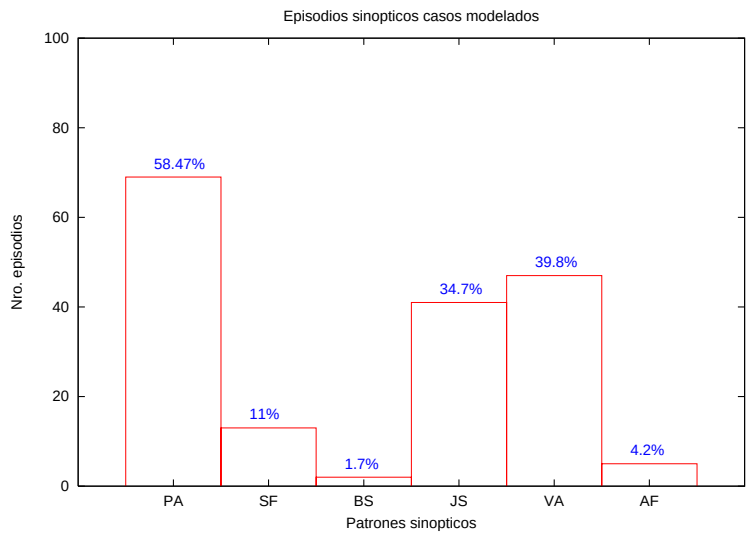

Figure 5.7: Synoptic episodes found during the period studied.

5.2 Seasonal Analysis

In order to differentiate the synoptic patterns during different times of the year, the events are separated seasonally into during of fall, winter, and spring (see Table 5.1).

E1	March - April - May
E2	June and August
E3	September - October - November - December

Table 5.1: Groups of synoptic episodes separated by seasons

Thus, we find the following distribution of episodes throughout the three groups defined.

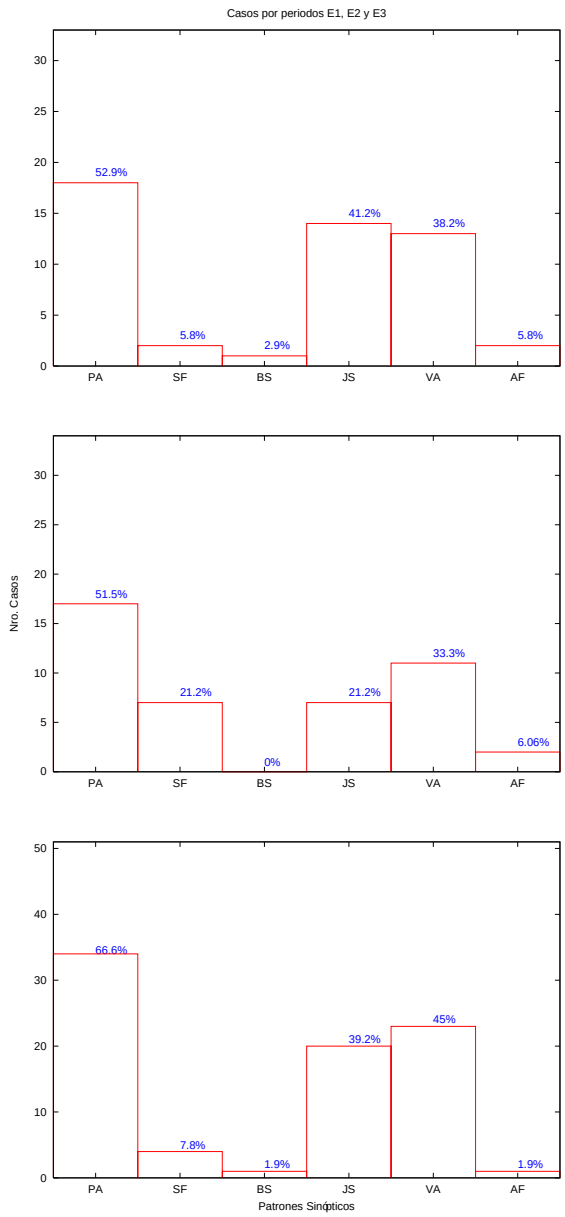

Figure 5.8: Synoptic episodes distributed in E1, E2, and E3 seasonal groups.

The anticyclonic predominance (AP) is present in a greater percentage in all of the periods in accordance with the climatology described in Chapter 2, where the anticyclone is described as a major regulatory factor of the climate in these latitudes. In the E2 group a greater presence of frontal systems that affect this area are present. Likewise, atmospheric instability is associated with these events. It

is important to note, the high percentage of high trough (HT) in every period. These events provoke instability as well as stability in a relatively short time, like during a night.

Chapter 6

Evaluation of the MM5 model

The validation of the MM5 modeling system was performed by contrasting the data from domain 4 of the model with the real (observed) data registered by the meteorological station at the summit of Macón. In order to do this, standar meteorological variables registered in situ are compared with simulated ones calculated at the same place and time by the MM5 model. The data output from the model has a frequency of one hour, thus they were compared with the data from the station between 00Z and 09Z. Therefore, the following variables were analyzed:

6.1 Temperature

The temperature at 2 meters over the surface at Macón registered by the meteorological station and that simulated by the MM5 model were compared. The data reflect that a relationship between the data exists, but it is concentrated below the line 1:1 (Figure 6.1). This means that the simulated data have lower values than those of the real data, but there exists a good correlation in their tendency. To quantify this relationship the BIAS error analysis was used, which calculates the error between forecasted data and data observed by using their difference (BIAS = forecasted data – observed data) [White et al, 1999]. A plot of observed versus forecast temperature can be seen in Table 6.1, here the results with a negative value indicate that the forecasted temperature data is less than the observed data. This can also be seen in the histograms showing the temperature data (Figure 6.2). While weather station temperature show an average around -2 ^{o}C, the modeled temperature show an average of -8 ^{o}C.

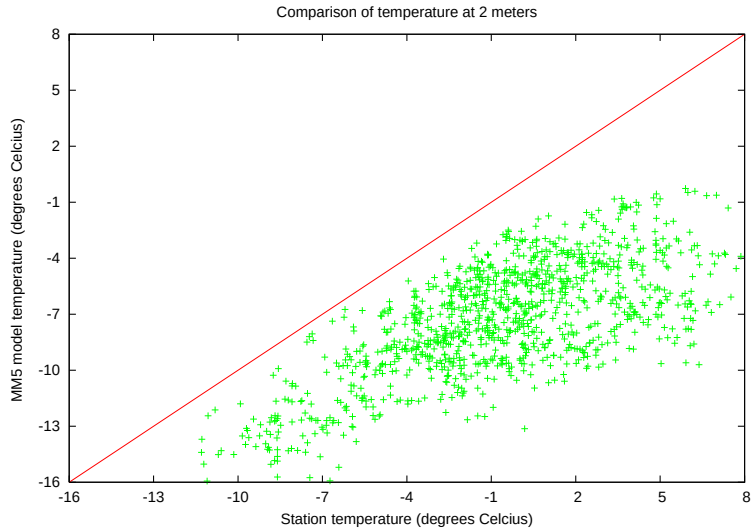

Figure 6.1: Comparison between simulated data of temperatures at 2 meters with observed data.

BIAS - Variable	Minimum	Maximum	Average	Median
Temperature 2m	-16.1	-0.54	-6.56	-6.12
Wind Int. 10m	-9.61	11.47	1.42	1.56
Relative Humidity	-23.41	38.71	10.11	9.46

Table 6.1: BIAS error analysis for the simulated data by MM5 and the data observed by the meteorological station at Macón.

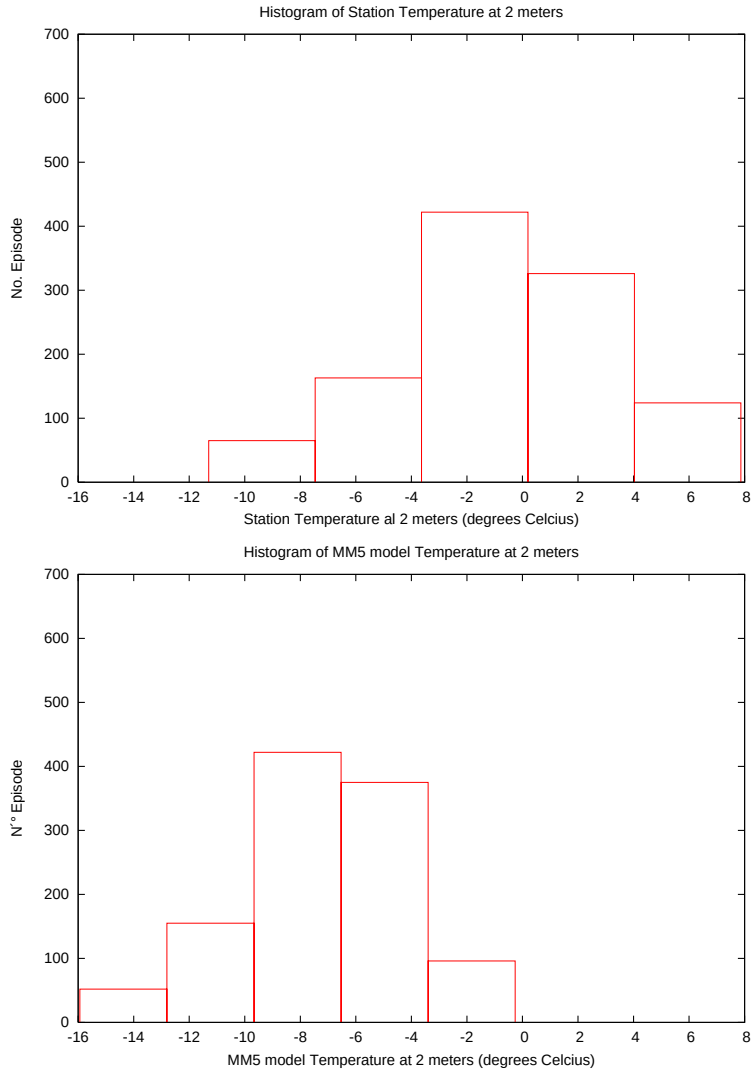

Figure 6.2: Histogram of the temperatures: above observed data; below simulated data.

6.2 Wind Speed

The magnitude of the wind is registered by the station at 10 meters over the surface of Macón and is compared to the data from the MM5 model at the same altitude. This shows a concentration of points above the line 1:1 (Figure 6.3), which indicates an overestimation of the model with respect to that observed. Table 6.1 shows the results of the BIAS error analysis, yielding positive values, which reflects this overestimation. The histogram of the data (Figure 6.4) shows that the station data and the model data have a the median around 5 ms^{-1}, but the observed values have a grates scatter.

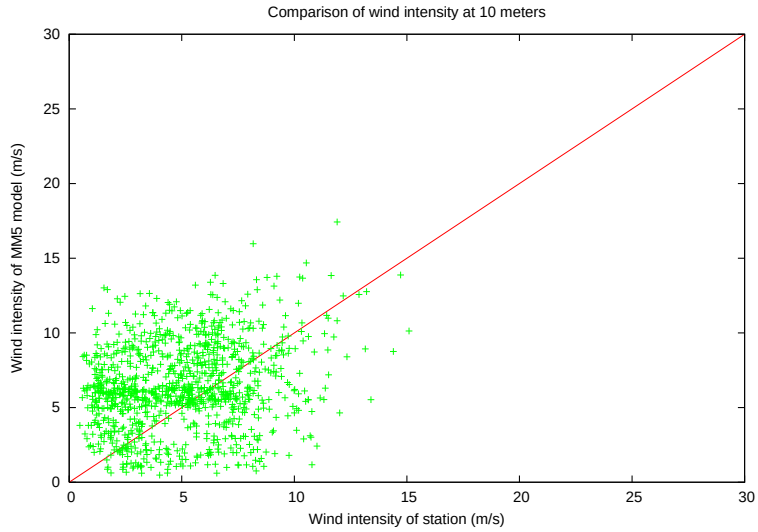

Figure 6.3: Comparison of the wind at 10 m from the surface of Macón observed by the station with those simulated by the model.

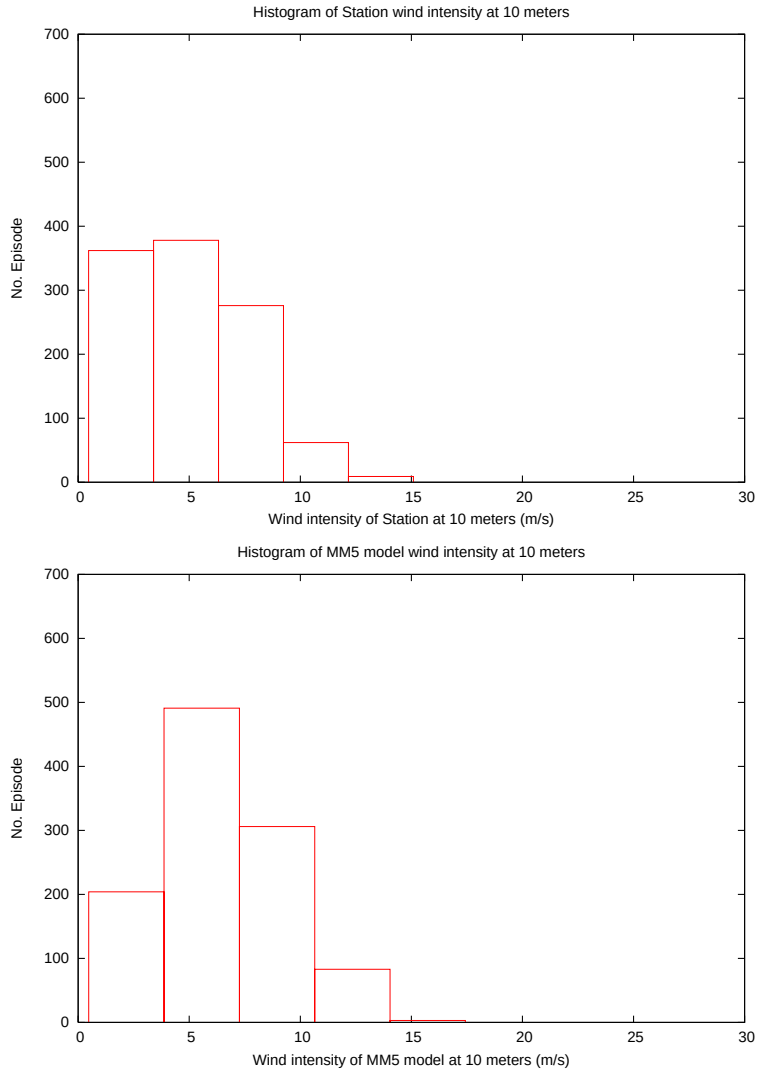

Figure 6.4: Histograms of wind intensity: above for the meteorological station; below for the MM5 model.

6.3 Humidity

The humidity sensor of the meteorological station has had problems in its calibration [privat comunication with Marc Sarazin], thus, its observed data is not correct and are not representative sample. This justifies the little variability and the pattern marked around 10% and 25%, which the figure 6.5 and figure 6.6 show. Under such conditions, it is impossible to validate the relative humidity that the model calculate.

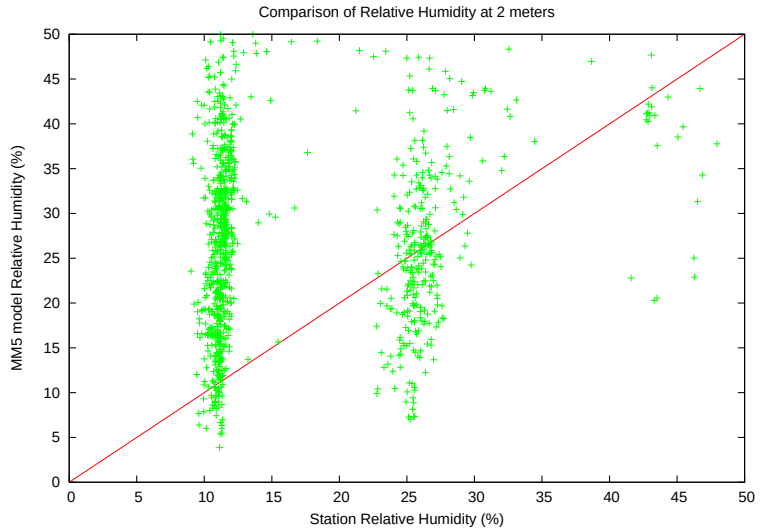

Figure 6.5: Comparison of relative humidity of the meteorological station in Macón and the MM5 model.

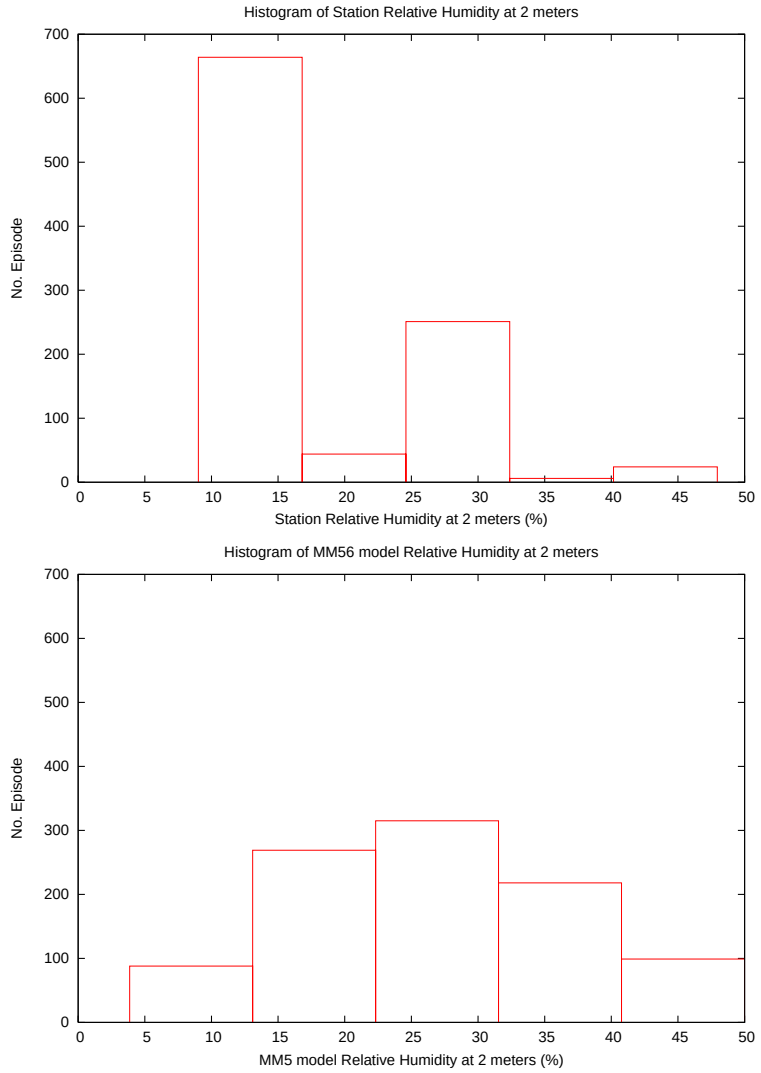

Figure 6.6: Histogram of relative humidity: above from the meteorological station; below from the MM5 model.

6.4 Analysis

In order to consider the errors of the model, it is important to take into account some relevant factors that affect the results. Mainly, it is the scarcity of the data in the zone and generally speaking, in South America, where the integration of real information by means of the global models is a boundary condition for simulations with the MM5 are minimum. Despite these difficulties, errors can be decreased using techniques to improve the forecasted data and the systematic errors that are found to be present

in the simulations can be lowered. One of the techniques used that yields good results is the application of the Kalman filter which in previous studies [Ramos, 2003; internet reference 2] has shown substantial improvements of the forecasted data.

Chapter 7

Trajectory Analysis

Trajectory analysis was done for the purpose of evaluating where the air flow during the night passing Macon comes from. Previous statistical studies of turbulence analysis show that the greatest contribution to seeing is produced by turbulence at lower levels near the surface [internet reference 4]. Considering this, trajectories were calculated that reach Macón, paying attention to those that start at levels lower than the Macón summit, especially, from the salt marsh of Arizaro, close to where the turbulence was registered by the MASS instrument. Also, we want to find out if the air flow that passes trough Paranal can arrive at Macón the same night, as well as find out if the seeing measured in Paranal is related to that observed in Macón. Therefore, trajectories from MM5 domains 2, 3, and 4 were calculated every night.

7.1 Paranal - Macón Trajectories

To find out if a relation exists between the airflow that passes trough Paranal and the airflow that reaches Macón a trajectory analysis was done, starting at Paranal (forward trajectories), continuing throughout the night (00Z to 09Z) and that that reaches Macón (backward trajectories) in the same period of time. This relation can be made since both sites are at very similar latitudes, trying to see if seeing events that are measured at Paranal can be transported toward Macón.

Greater importance was given to the trajectories that flow from Paranal from 0.5 km and 1 km of altitude above the surface. This was also done for Macón from 0.5 km and 1 km, since these levels, based on previous analysis [internet reference 4], is where the greatest amount of turbulence contribution for seeing is produced.

Next, by studying each case, it was found that only during two nights the air that flowed from Paranal passed trough Macón (Figure 7.1). This corresponded to June 11, 2005 and November 19, 2005. From this, it was found that the airflow that passed at the levels close to the surface is not capable to travel in one night passing the Andes mountain altitude range from Paranal to Macón. In these cases, a relation having a common meteorological pattern cannot be found, due to the fact that on June 11 there were a frontal system episode and on November 19 there was a jet stream present. It is important to consider though, that for both cases wind speed intensity should be high so that the air is capable of traveling the same night from Paranal to Macón.

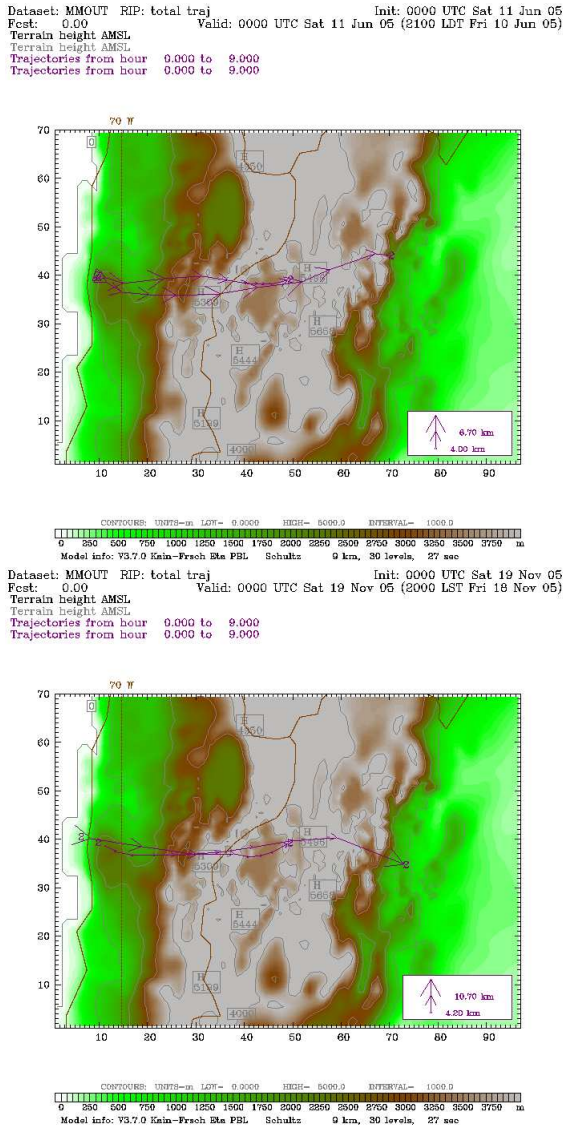

Figure 7.1: Trajectories from Paranal to Macón. Abobe airflow traveled from 00Z to 09Z for June 11, below: November 19.

7.2 Trajectories that reach Macón

The analysis of the airflow that reaches Macón was done with backward trajectories from 00Z to 09Z. To calculate this, domain 4 was used preferablly, but there are cases in which the velocity of the wind did not allow the trajectory found in the domain to be calculated. In this case, the data from domain 3 was used. Analyzing the trajectories that arrive at the surface of Macon (4.600 m.a.s.l.) and 1/2 km of altitude (5.000 m.a.s.l.), it was found that the wind velocity in 97% of the cases has a West component.

There are differences between the air that reaches the surface at Macón and an altitude of 1/2 km. This can be seen in Table 7.1 where the arrival of airflow is distributed quite homogeneously between the directions from the NO - O - SO in the case of the 1/2 km of altitude over Macón. This is different from the airflow that reaches the surface, which come mainly from the NO - O.

	N	NO	O	SO	S	SE	E	NE
Surface	1%	43%	33%	21%	1%	2%	0%	0%
1/2 km Altitude	1%	31%	37%	30%	2%	2%	0%	0%

Table 7.1: Trajectory directions that reach Macón at the surface and at an altitude of 1/2 km.

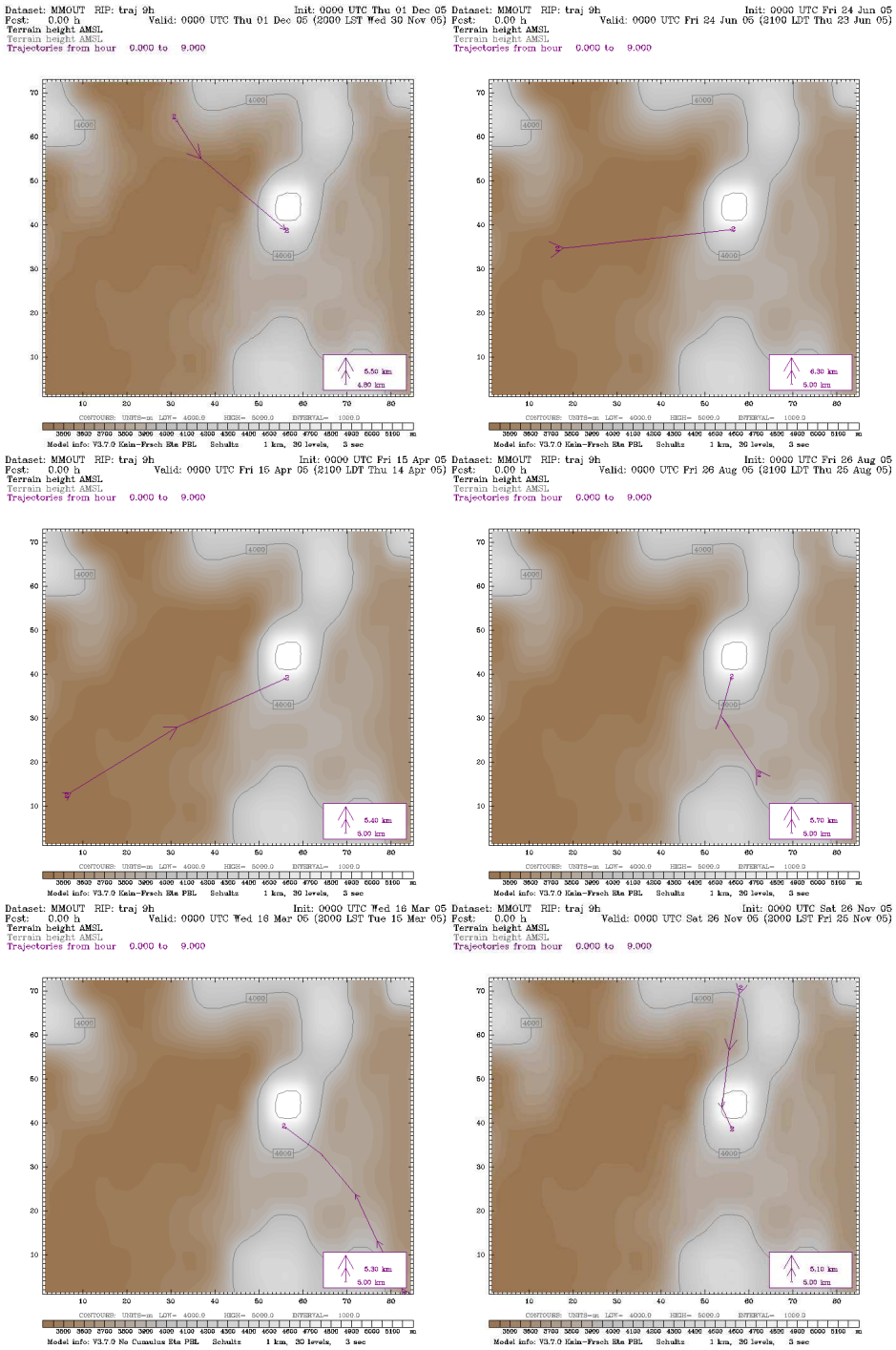

Figure 7.2: Trajectories that reach Macón. From top to bottom and from left to right the trajectories are considered from: NO, O, SO, S, SE, N.

7.3 Analysis of altitude traveled by the trajectory

The purpose of analyzing the altitude of the trajectory (air flow) is to see the influence that the salt marsh of Arizaro has over the flow pattern and if the turbulence from low levels can ascend slope up and reaches Macón.

It was found that over 90% the trajectories do not travel from low levels to the summit of Macón. The airflow that reaches the summit of Macon come from altitudes over 4.500 (m.a.s.l) and the airflow that passes trough over Macon come from altitudes in the range of 5.000 to 5.500 (m.a.s.l.) for 1 km over the summit. Over 90% of the trayectories cases was there and influence from lower levels, and 5 of which the wind direction comes from the northeast, 2 from the west and 2 from the southeast. Thus, the contribution of turbulence from lower levels from Tolar that reaches Macón is almost null. The reason of this behaviour is that in Arizaro's salt marsh a secundary circulation (cell) is formed and stay during the night. This circulation is controled by the high of the thermal invertion layer, and does not allow for flow exchange forward higher altitudes. This secondary circulation is clearly seen in the latitudinal – vertical cross section profile above Macón and the salt marsh of Arizaro. Most of the wind that arrives is from the west and northeast and does not interact with the surface levels of the salt marsh at Arizaro.

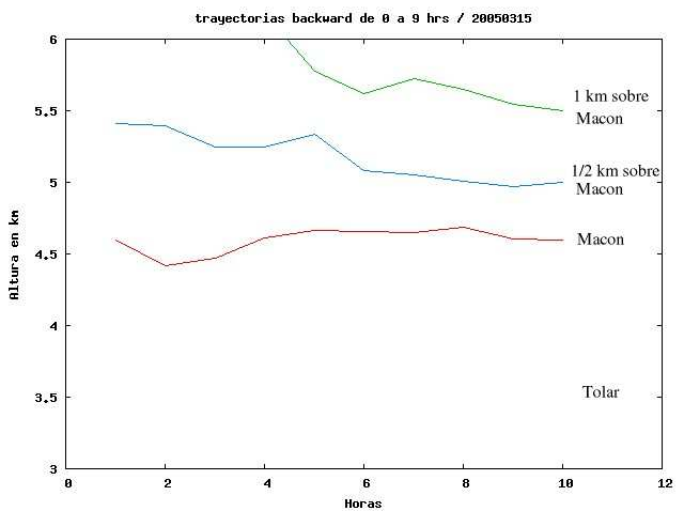

Figure 7.3: Altitude traveled by trajectories in one night. Air that reaches the top of Macón (4.6 km), 0.5 km above the summit (5 km) and 1 km above the summit of Macón (5.5 km), for the night of March 15, 2005.

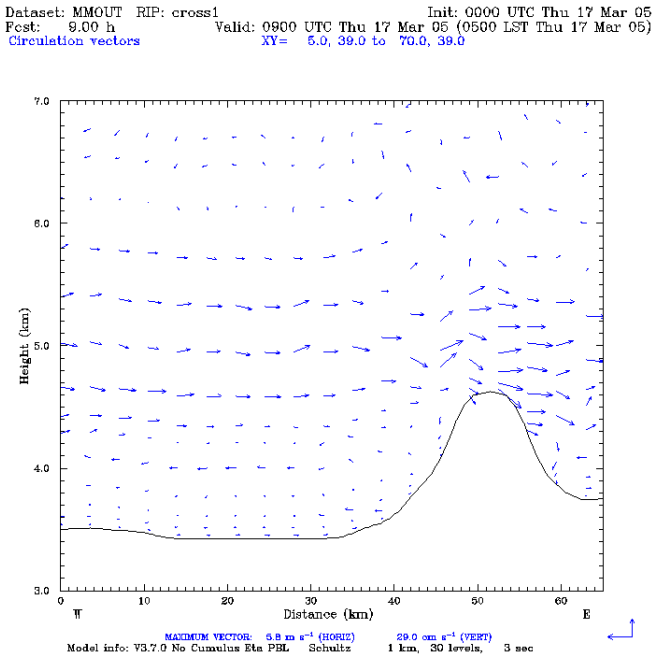

Figure 7.4: Vertical profile above the latitude of Macón, wind velocity in vectorform.

Chapter 8

Seeing Statistics

In this section we show the results of a statistical analysis was done of the seeing data. The campaigns were done using the MASS instrument which yields information about turbulence and seeing from 0.5 km over the surface of Tolar. To estimate the seeing at Macón, the following criteria were considered:

1. The record were taken at the station located in Tolar (3,500 m.a.s.l.) one kilometer lower than the summit of Macón (4,600 m.a.s.l.).

2. The trajectory analysis (chapter 7) showed that the airflow that arrives to Macón is not influences by lower levels at the Arizaro salt marsh.

3. The airflow that reaches Macón during one night is not related with the airflow that comes from Paranal.

Consequently, to infer the seeing of Macón, these criteria imply that in a first approximation, the seeing (here after seeing2) can be obtained using the measurements of C_{n}^2: with the MASS instrument at Tolar from 2 km and higher, that is to say:

$$seeing2 = ((C_{\mathrm{n}3}^2 + C_{\mathrm{n}4}^2 + C_{\mathrm{n}5}^2 + C_{\mathrm{n}6}^2)/6.8e-13)^{0.6}$$

where $C_{\mathrm{n}3}^2$ corresponds to the level at 2.0 km and $C_{\mathrm{n}4}^2$, $C_{\mathrm{n}5}^2$, $C_{\mathrm{n}6}^2$ corresponds to the levels at 4, 8 and 16 km respectively.

The seeing and turbulence database has a total of 42672 records.

8.1 Distribution Form

To know the form that the data are distributed, we used a boxplot scheme. A boxplot is a graph with 5 measurements from bottoms to top: relative minimum (inferior extreme of the previous tail of the first quartile), the first quartile (25% of the data), the second quartile or median (50%), third quartile (75%), and the relative maximum (superior extreme of the posterior tail of the third quartile). The data above the relative maximum (circles) corresponds to the extreme values or "outliers" measured using cut off points for this purpose. In Figure 8.1 an abundance of extreme values can be observed.

The objective of this summary is to calculate the quantity of these extreme values and show the cut off points that individualize the extreme values or outliers.

The cut off points separate the data that, due to its distance from the central measurements (median), are strangely distributed. We found two superior cut off points that mark two sectors, one

being of moderate outliners (values not so distant) between the first threshold and the second; and severe outliers beyond the second threshold.

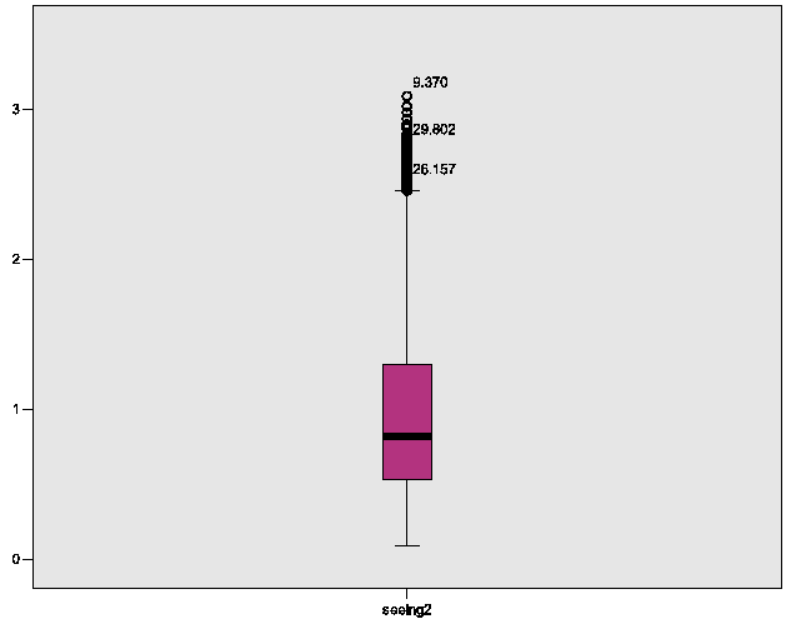

Figure 8.1: Boxplot for the seeing data.

The boxplot of the data (Figure 8.1) shows an asymmetric distribution, the right side having a great amount of outliers.

Table 8 .1 shows the summary measurements of the seeing data.

Data	valid	43672
	missing	0
Mean		0.956
Median		**0.821**
Std. deviation		0.528
Variance		0.279
Minimun		0.09
Maximun		**3.09**
Percentil	25	0.532
	50	0.821
	75	**1.302**

Table 8.1: Statistic information of seeing data.

The seeing data range is between 0.09 and 3.09. The average is 0.96, the median is 0.82 and 75% of the measurements are at most 1.30.

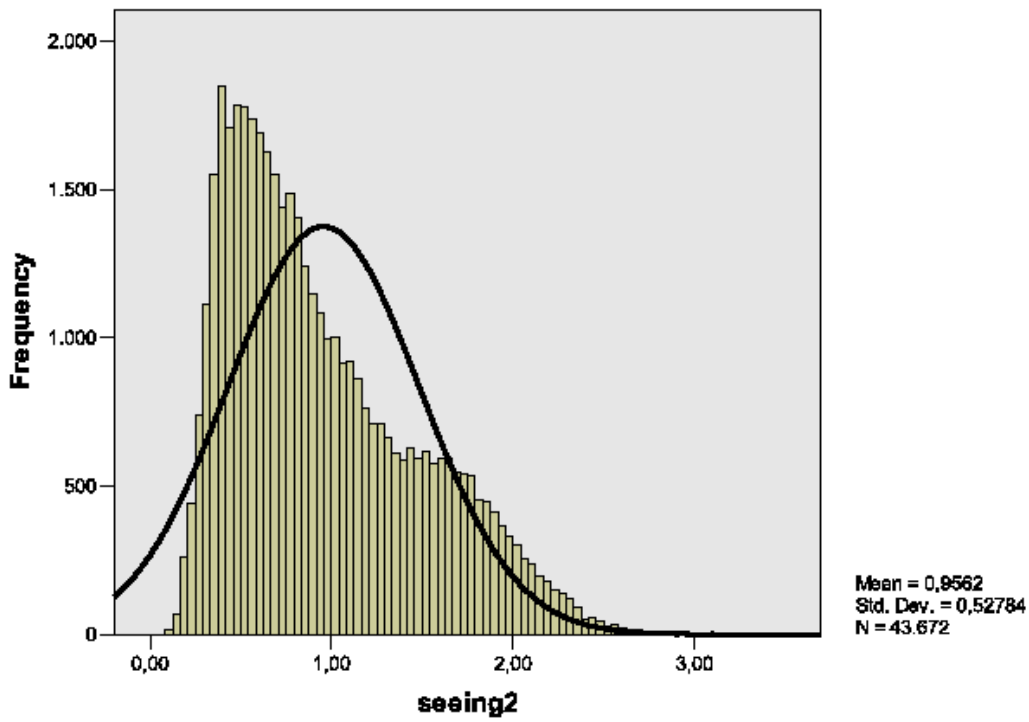

Figure 8.2: Histogram and distribution of the seeing2 data.

In the histogram of seeing (Figure 8.2) the asymmetry is clearly observed, but also something that seems to be two different groupings; one that is very asymmetric with a maximum nearing the value of 0.5 of seeing and the other with a maximum around 1.7.

8.2 Seeing $\leq$ 1

In this section we studied the cases that have a value of seeing2 less than 1. This values was chosen because empirically it is a value that limits the *good* and *bad* seeing. Furthermore, it is close the average value of distribution that is 0.956. Table 8.2 shows the number of cases with seeing2 lower than 1. Here 61.2% of the data have seeing2 less that 1 and corresponds to 77 nigths of the sample of 126 nigths that were measured in Tolar. According to this criterion, the remaining 38.8% of the measurements had a

seeing2 greater than one. Concerning the number of nights this 38.8% of measurements corresponds to 109 nights (of 126), where a seeing2 was measured at > 1. This tells us that mostly there are no complete nights with nigths less than one in Macón. This conclusion can be observed in Figure 8.3, which shows each night measurement percentages with seeing2 greater or less than one, where in almost every day there is a portion of seeing2 > 1 (in pink).

	Frequency	Percent	Valid Percent	Cumulative Percent
Hasta 1	26728	61.2	61.2	61.2
Más de 1	16944	38.8	38.8	100.0
Total	43672	100.0	100.0	

Table 8.2: Table of seeing2 categorized by values greater or less than one.

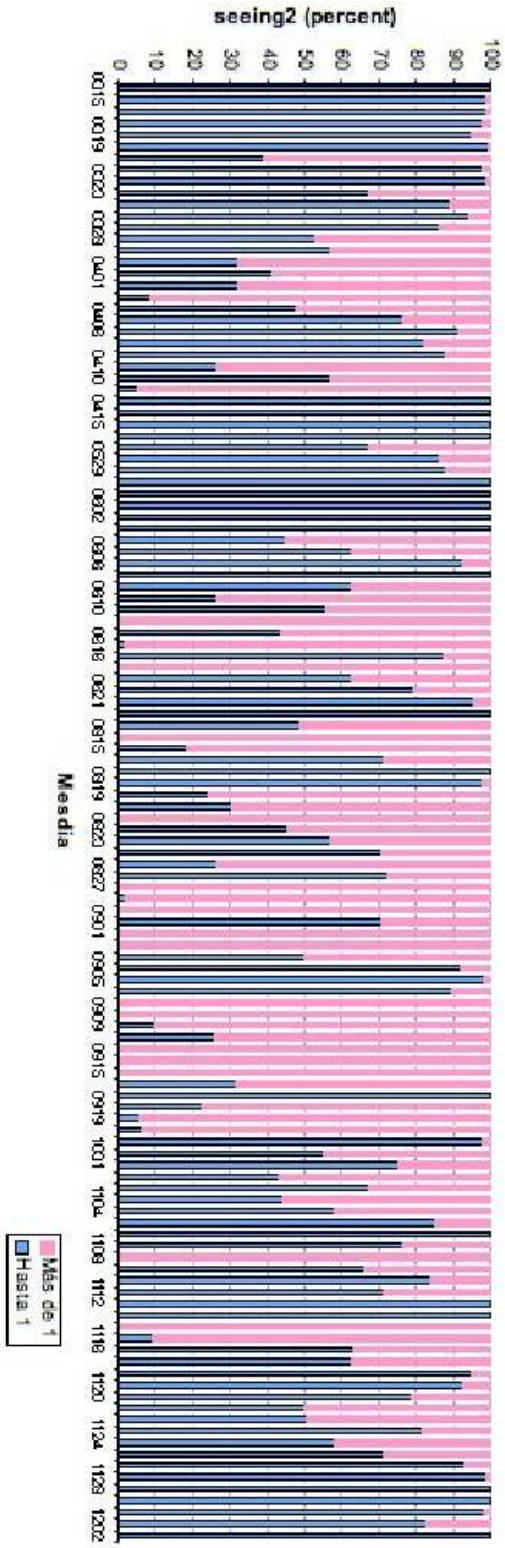

Figure 8.3: Nights with seeing2 measurements greater (pink) or less (blue) than one.

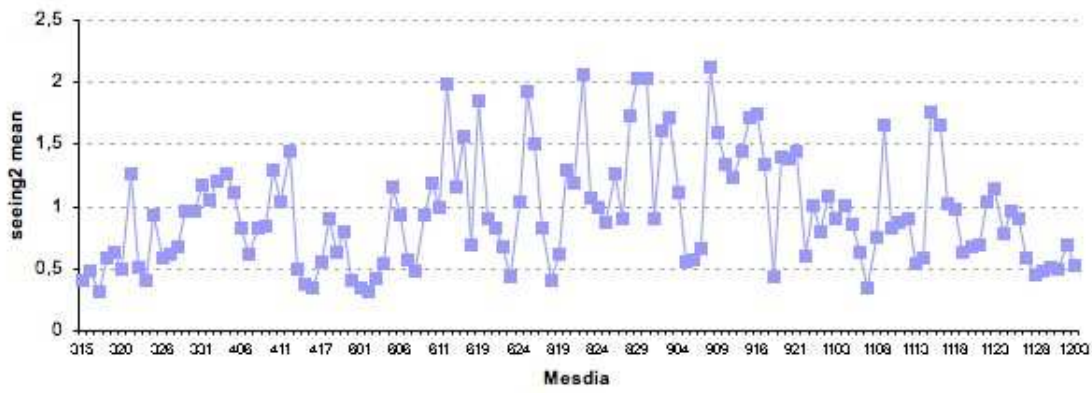

Figure 8.4: Average seeing per night.

In figure 8.4 the seeing2 average for each night is ploted. The average values vary between 0.31 and 2.13. The highest are found between June and September and the lower mostly in the summer.

8.3 Study of superior outliers (extreme superior values)

Due to the asymmetry of the distribution function of the data (Figure 8.2), we did a study of outliers with the purpose to know the influence these have in global behavior of seeing2 above Macón.

8.3.1 Limits for the superior outliers

Table 8.3 shows the superior level.

Superior limit 1 (ls1)	2.46
Superior limit 2 (ls2)	3.61

Table 8.3: Superior level of outliners.

Between 2.46 and 3.61 the superior moderate outliners can be found. The data with seeing $>$ 3.61 corresponds to severe outliers (superiors).

The answer to the question. How much data is there with seeing $>$ ls1 (2.46)? is shown in Table 8.4 where the percentage of outliers is to minimum and corresponds to a 0.4% and to 13 nigths of the total 126 nigths. Table 8.5 shows in detail these 13 days.

Seeing2	Frequency	Percent	Valid Percent	Cumulative Percent
< 2.46	43484	99.6	99.6	99.6
≥ 2.46	188	0.4	0.4	100.0
Total	43672	100.0	100.0	

Table 8.4: Table of greater and lesser values at the ls1 limit.

Month-day	< 2.46	≥ 2.46	Total
0411	391	7	398
0613	420	2	422
0815	323	1	324
0816	434	7	441
0822	414	9	423
0829	**196**	**76**	**272**
0830	415	6	421
0903	299	1	300
0908	**154**	**68**	**222**
0916	400	1	401
0916	345	3	348
1116	126	5	131
1118	260	2	262
Total		188	

Table 8.5: Month – night that corresponds to outliers of the seeing2 variable.

The nigths with a greater quantity of superior outliers were the 29 of August (40.4% of the total and 27.9% of the measurements of the nigth) and the 8 of September (36.2% of the total and 30.6% of the measurements of the nigth). The remaining nigths represent 23% of the outliers.

What nigths correspond to the values of seeing2 $>$ ls1 (2.46)? The nigths with outliers of greater magnitud were: $11/04/05, 29/08705$ and the $08/09/05$, which can be observed in the boxplot of seeing2 for the nigths with extreme values (Figure 8.5).

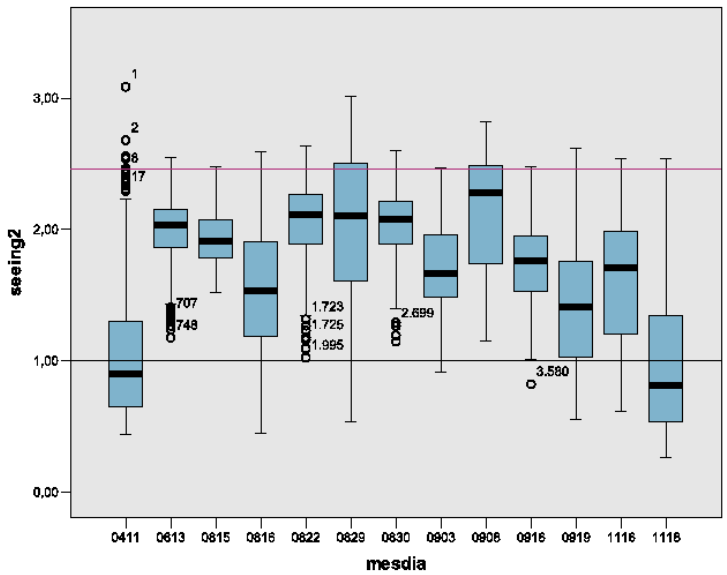

Figure 8.5: Boxplot of seeing2 on nights with outliers.

And for each nigth, what is the maximum seeing2 value? Figures 8.6 and 8.7 show the maximum seeing value per nigth, as well as the maximum value and the median respectively.

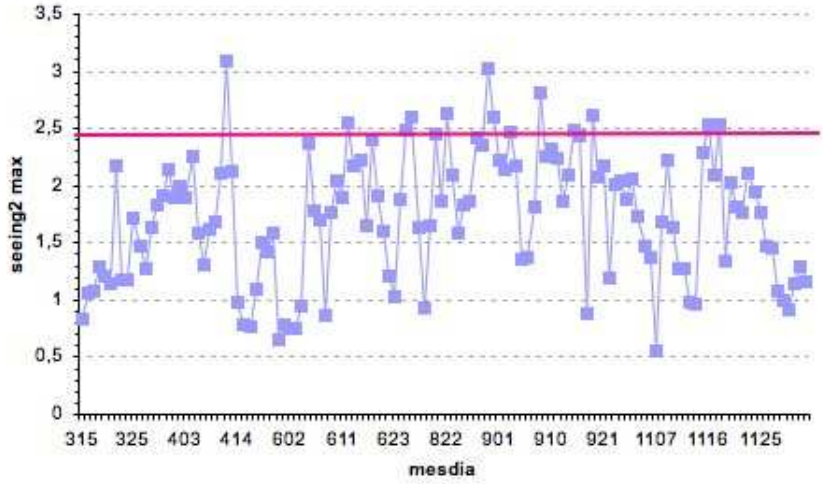

Figure 8.6: Maximum seeing2 per nigth.

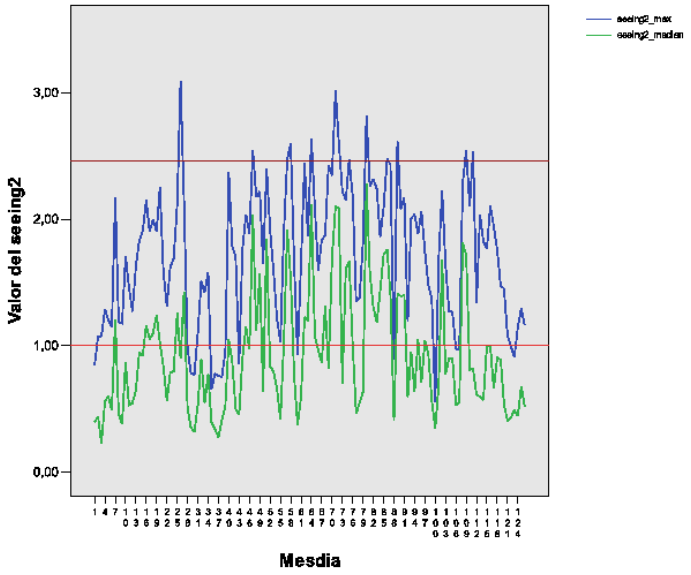

Figure 8.7: Maximum and median seeing2 per nigth.

8.4 Seeing2 study for periods of 2 hours

The data is divided by nigth and at every 2 hours. Figure 8.8 shows that the median (wide line in each boxplot) of seeing drops as the night progresses.

Just as with the maximum values of seeing2, Figure 8.9 shows the minimum, median, and maximum of seeing2 per hour.

We conclude that the seeing2 decay during the night and the most probable reason for this is due to the cooling of the atmosphere.

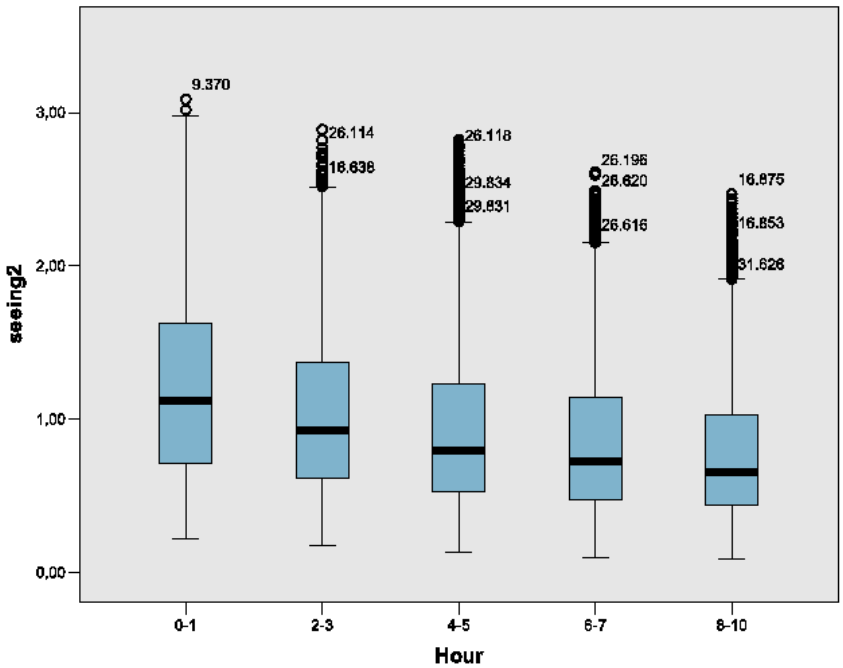

Figure 8.8: Boxplot every 2 hours for every night.

8.5 Accumulated frequencies of seeing

Figure 8.10 show accumulated frequencies of seeing2 at Macón. This, when compared to other astronomic sites (Figure 8.11) shows that the bad seeing has greater frequency in Macón. If we evaluate the value of seeing = 1 in Figure 8.11a and 8.11b, we see that in Macón this value is less reoccurring than at other astronomic sites, and observing the curve there are greater values of seeing accumulated in Macón.

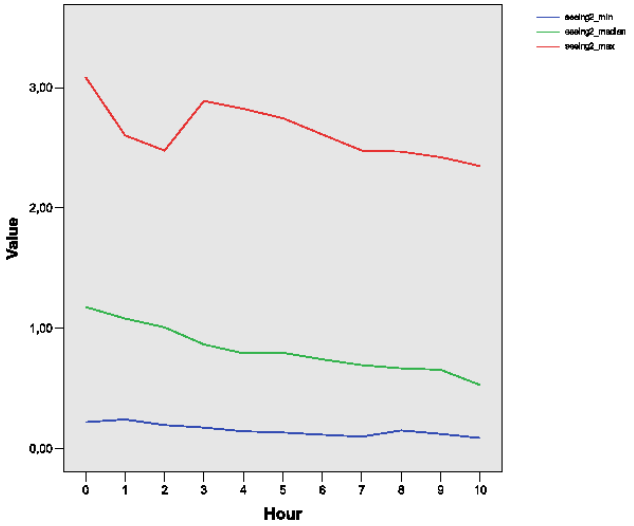

Figure 8.9: Minimum, maximum, and median for seeing2 per night.

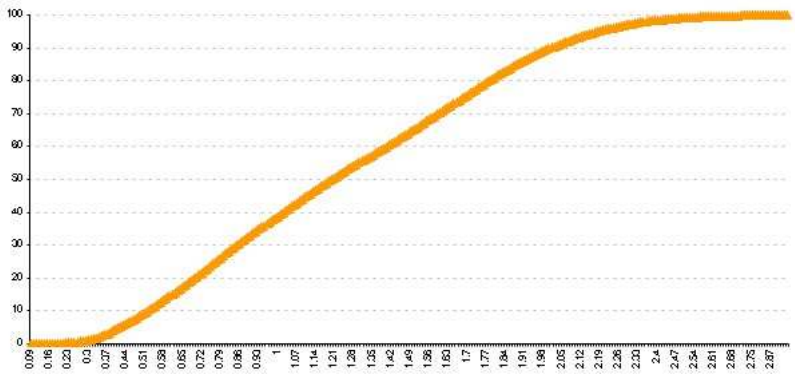

Figure 8.10: Accumulated percentages of seeing2.

a)

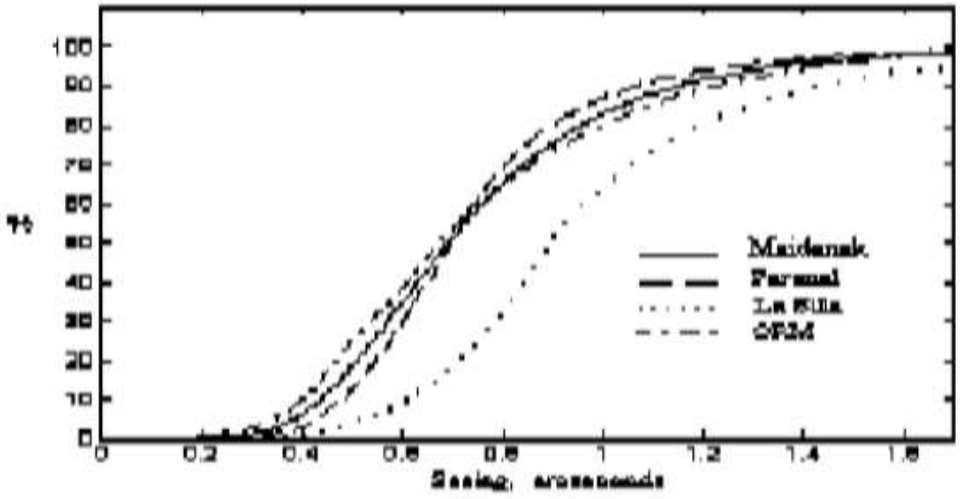

b)

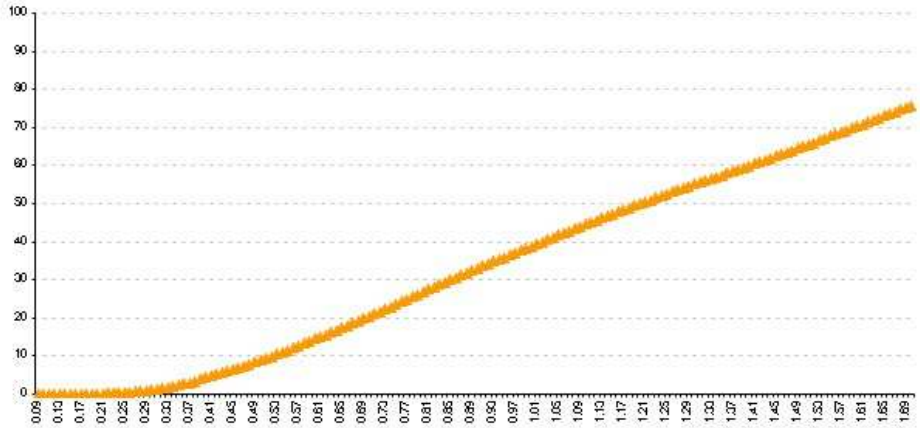

Figure 8.11: Accumulated frequency of seeing for different astronomic sites (above) and accumlated frequencies of seeing2 for Macón (below) compared with the same scale.

Chapter 9

Seeing Study

In this chapter the results of the search for a relationship between synoptic patterns and *good* or *bad* seeing are shown. For this purpose the previous studies (Chapters 5, 7 and 8) of seeing for Macón and for Tolar were used.

The statistical study previously done for Macón, where the first 2 levels of the turbulence entries taken with the MASS instrument in Tolar to calculate the seeing were not considered, served as a base for the classification of good and bad nights of seeing.

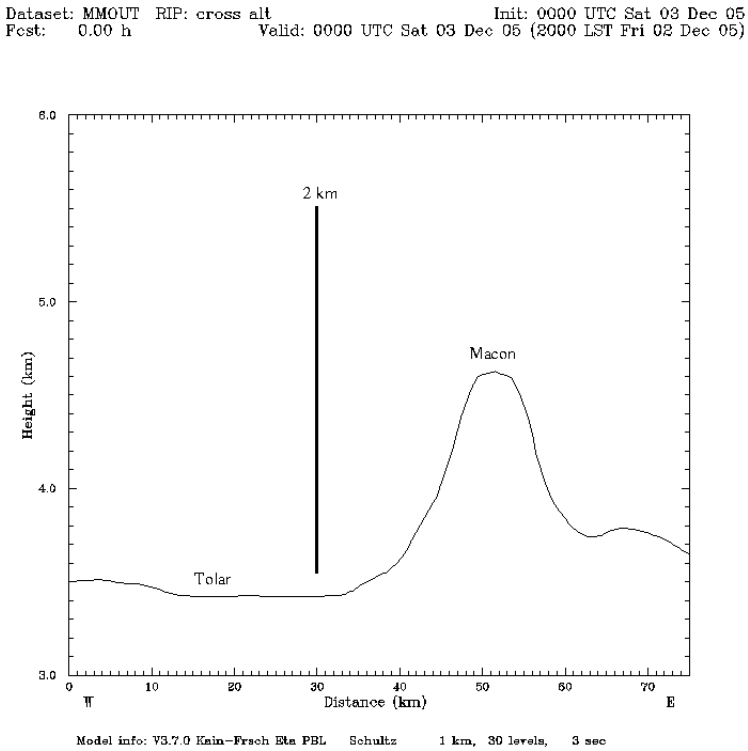

Figure 9.1: Altitude differences between Macón and Tolar, nivel at which the seeing is calculated.

9.1 Classification of seeing

To classify the seeing in Macon, we applied the clasification used in Paranal, proposed Julio Navarrete [internet reference 3], which is based on the adaptive optic. Table 9.1 show the classification of seeing byeand adaptive optic used for these cases.

Range	Type	Adaptive Optic
< 0.5”	Super	System of adaptive optic, maximum diffraction, excellent
		image quality with normal instruments
0.5”$<$ 0.8”	Good	Adaptive optic works well, infrared instruments (20
		microns) as VISIR accomplishes diffraction limit
0.8” $<$ 1.2”	Default	
1.2”	Bad	The adaptive optic begins to have problems correcting
		the atmosphere

Table 9.1: Classification of seeing based on adaptive optic.

9.1.1 Seeing at Tolar

Using these ranges to classify the seeing (using all levels of C_{n}^2) for the data at Tolar and using the median of each night, it was found that 3% of the cases were *good* and 47% if the cases were *bad* (Table 9.2).

Seeing	Super	Good	Default	Bad	Total
Casos	4	31	32	59	126
%	3%	24.6%	35.4%	47%	100%

Table 9.2: Clasification of seeing for Tolar, seeing calculated using all the turbulence measurement levels.

9.1.2 Seeing at Macon

The same statistical study of seeing2 for Macon, where the first two turbulence levels were not considered in the calculation.The bad cases are reduced to 24% and the good cases increase to 18% (Table 9.3).

Seeing	Super	Good	Default	Bad	Total
Casos	22	37	37	30	126
%	18%	29%	29%	24%	100%

Table 9.3: Clasification of seeing2 for Macón, not considering the first two levels of the turbulence data.

9.2 Isotherm 320 K

A way of relating the good and bad seeing with meteorological condition was to perform a vertical analysis of wind velocity and potential temperature. Our preliminary analyses [Report I and II previous to this study, internet reference 4] had suggested to related seeing to thermal thickness (see figure 9.2).

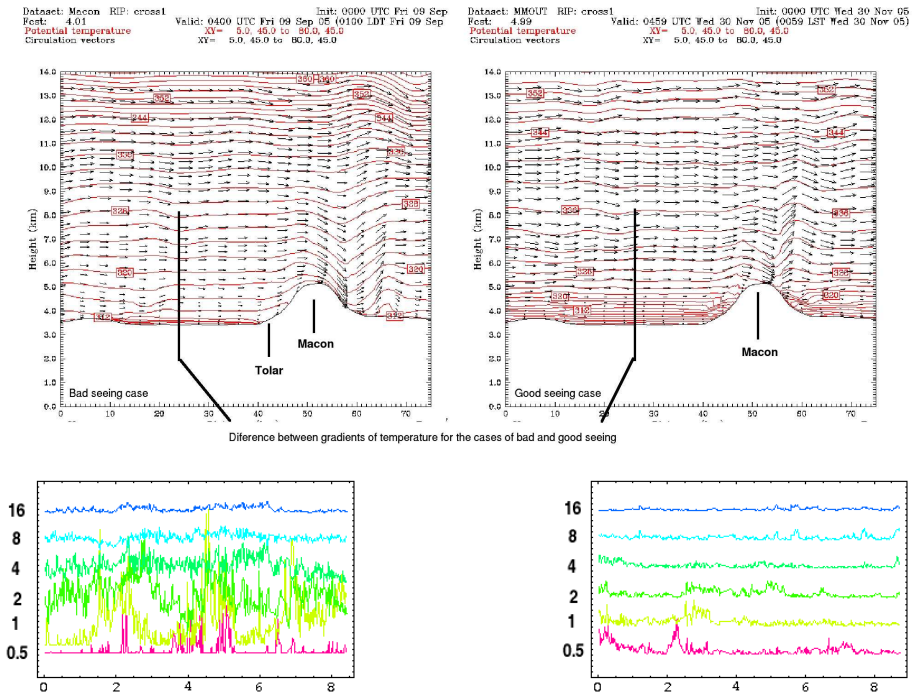

Figure 9.2: Comparison between a case of *bad* seeing and *good* seeing. Above, vertical cut of potential temperture (red lines) and wind velocity (vectors), the vertical black bars show the altitude difference of the isotherms (thermal thickness) between a case of high turbulence (lower left) and low turbulence (lower right).

Analizing figure 9.2 we conclud that the seeing is related to the vertical distance between isotherms. The higher is this distance, the high is the vañue of the seeing.

We decided to analize the altitud of the isotherm T = 320 K bacause the Macon summit high lies in the range of altitude of this isotherm. Figures 9.5 and 9.6 show two cases of *good* seeing and *bad* seeing and the altitude of the isotherm 320K. This suggests that there could be a relationship between thermal thinkness (vertical distance between isotherm) and seeing, but analyzing the mean value of seeing and the altitude of the isotherm per night this relationship was not found (Figure 9.4).

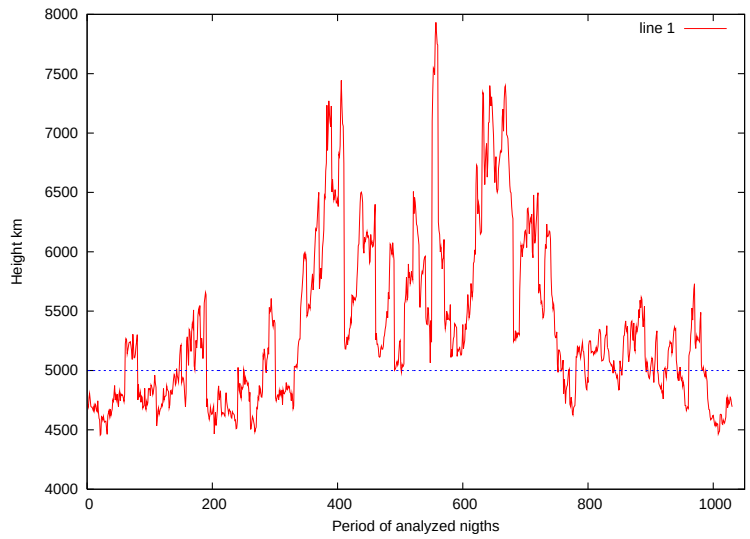

Figure 9.3: Average altitude of the isotherm 320K.

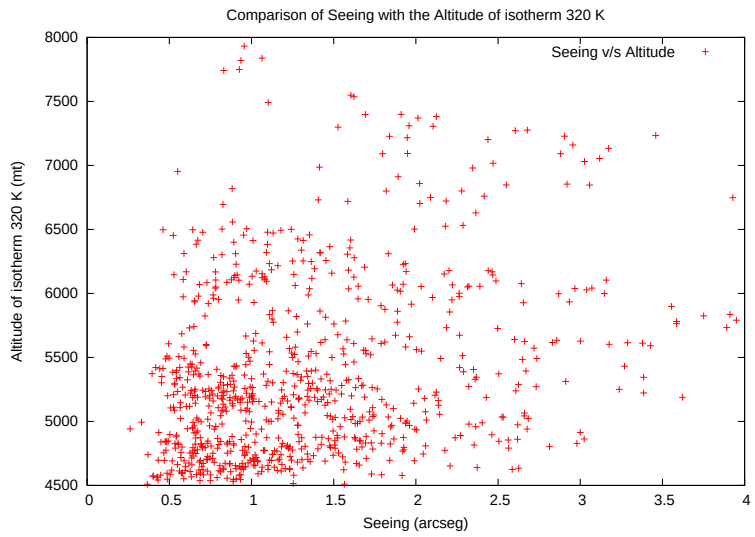

Figure 9.4: Seeing versus altitude of isotherm 320K.

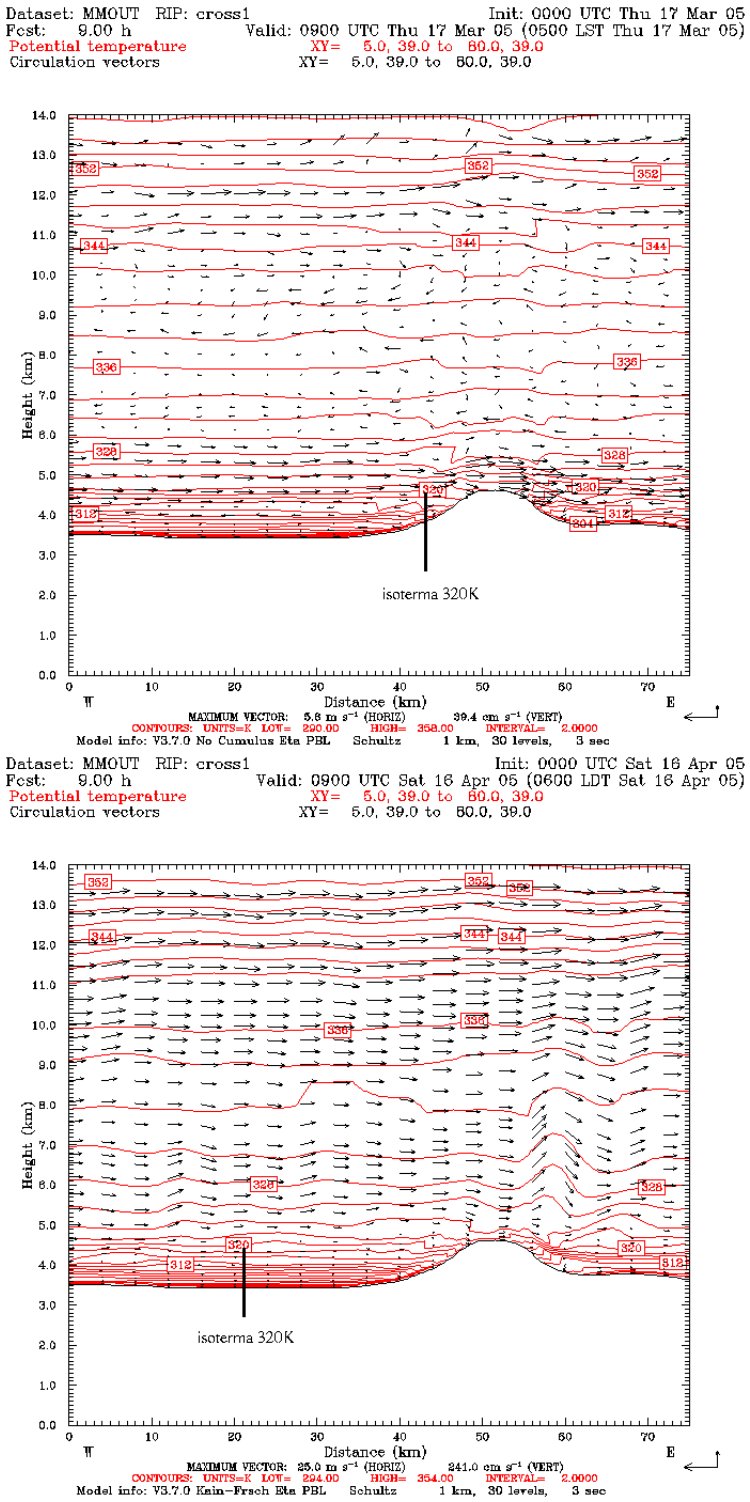

Figure 9.5: Altitude of isotherm 320K for cases of good seeing.

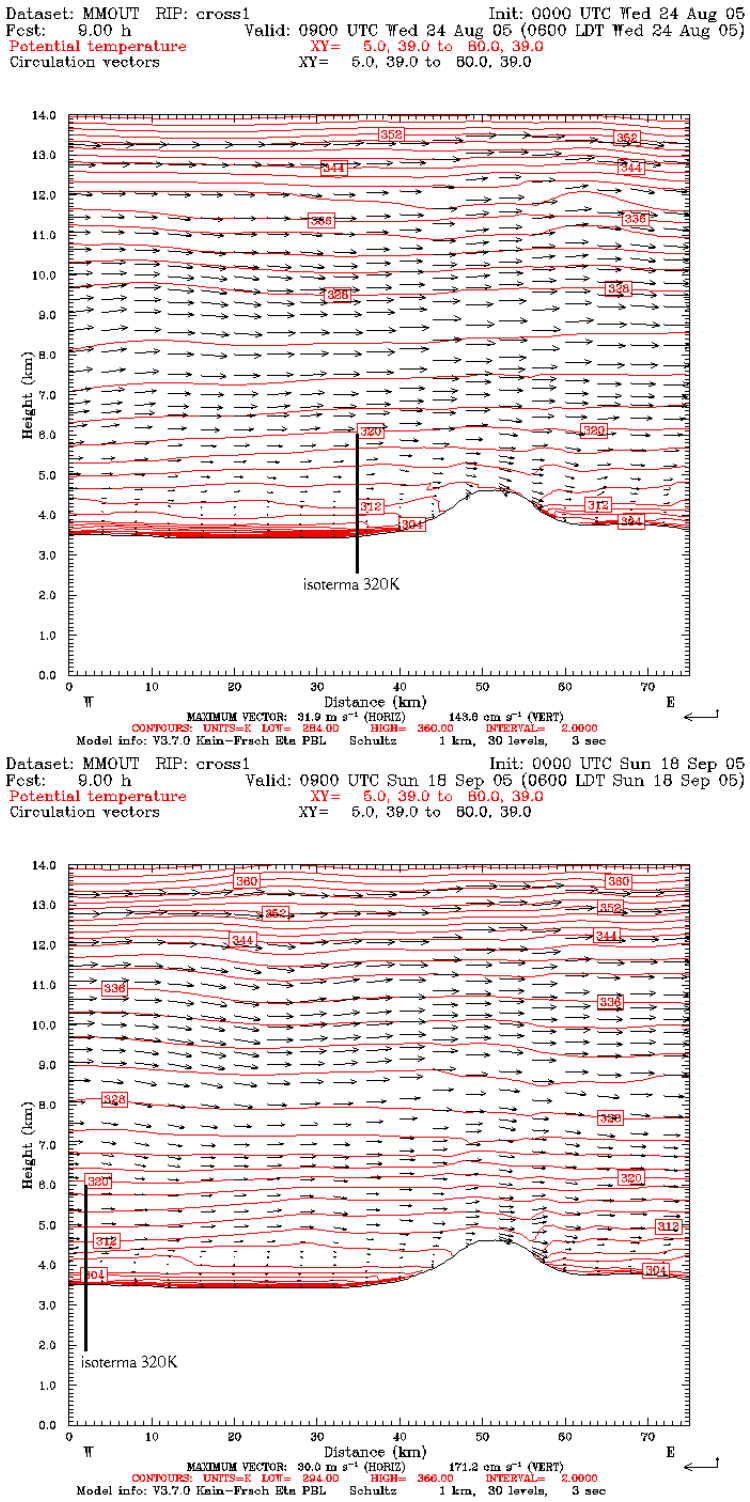

Figure 9.6: Altitude of isotherm 320K for bad seeing.

9.3 Seeing and wind

The wind velocity registered at 10 m of altitude by the meteorological station at Macón was compared with the seeing classification from section 9.1. These entries show that the predominate wind direction in Macón is from NW –W – SW and relating it with seeing it can be found that for the classification super (seeing < 0.5") the wind mostly has a direction between 270° and 345° (W – NW) with intensities less than 8 ms^{-1} . For episodes of seeing *default* (0.8" $<$ seeing $<$ 1.2") and *bad* (1.2" $<$ seeing) the direction of the wind in mostly concentrated between 240° and 135° (SW-S-SE) with intensities greater than 6 ms^{-1} (Figure 9.7).

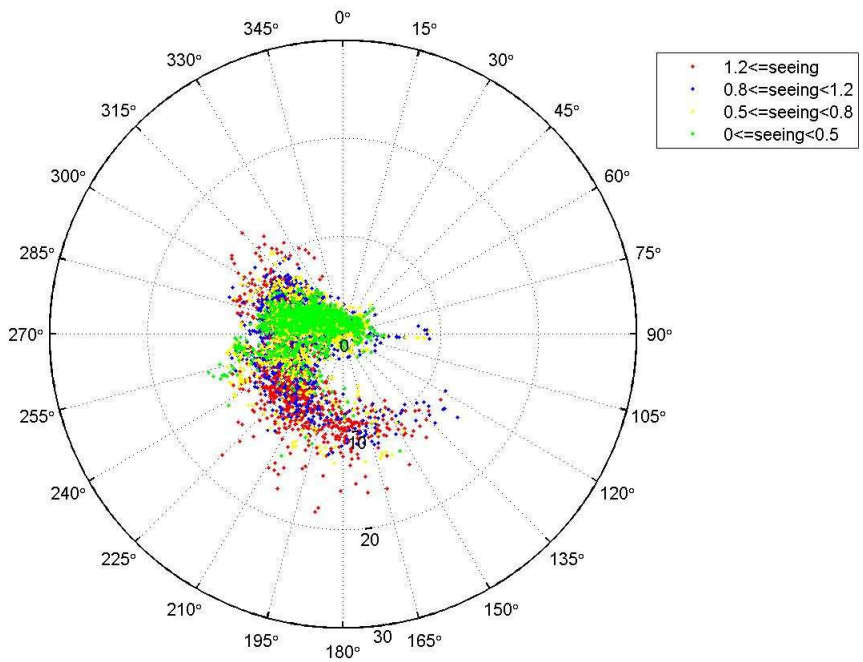

Figure 9.7: A winds compass rose compared with classified seeing.

The histogram of the wind direction shows that the wind on average has a direction between 220° and 290° (SW – W – NW) (Figure 9.8). Referring to wind intensity the histogram shows that the average of wind is 6 ms^{-1} (Figure 9.9).

Seasonally the wind rose for winds for the group E1 (Table 5.1) show that the wind is comming from the northwest (NW) direction with average intensities of 8 ms^{-1}(Figure 9.10).

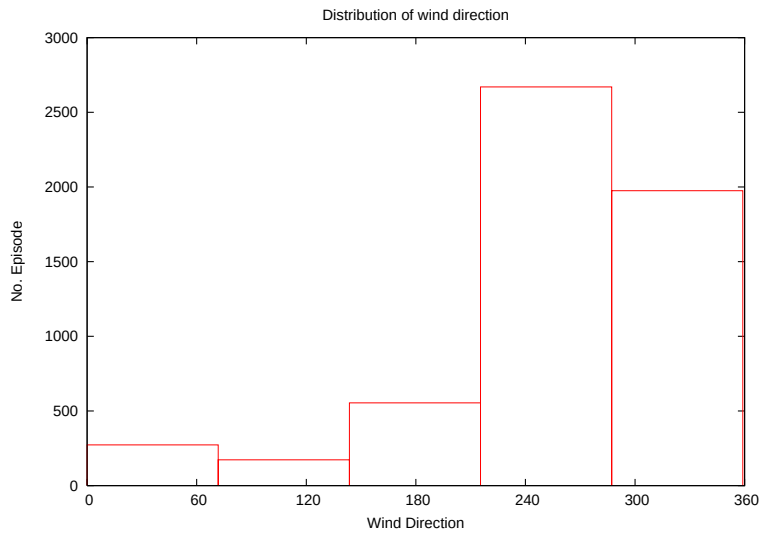

Figure 9.8: Histogram of wind direction for the Macón station for the period analyzed (March to December).

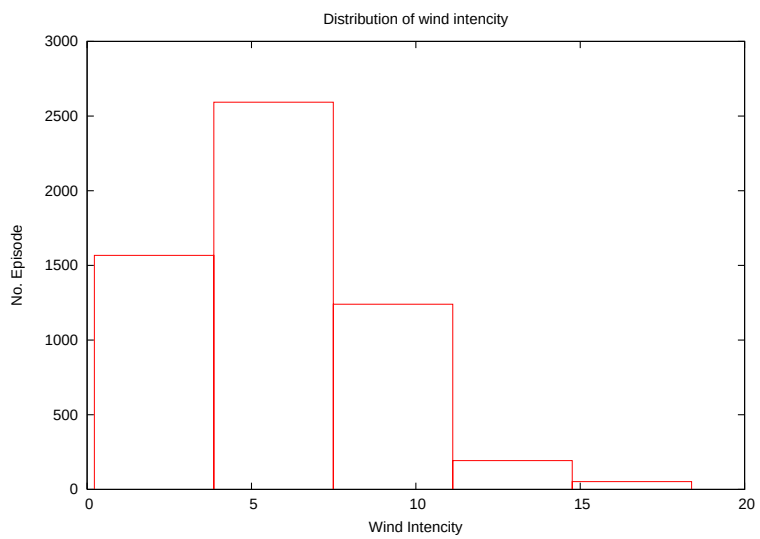

Figure 9.9: Histogram of the wind speed for the Macón weather station for the period analyzed (March to December).

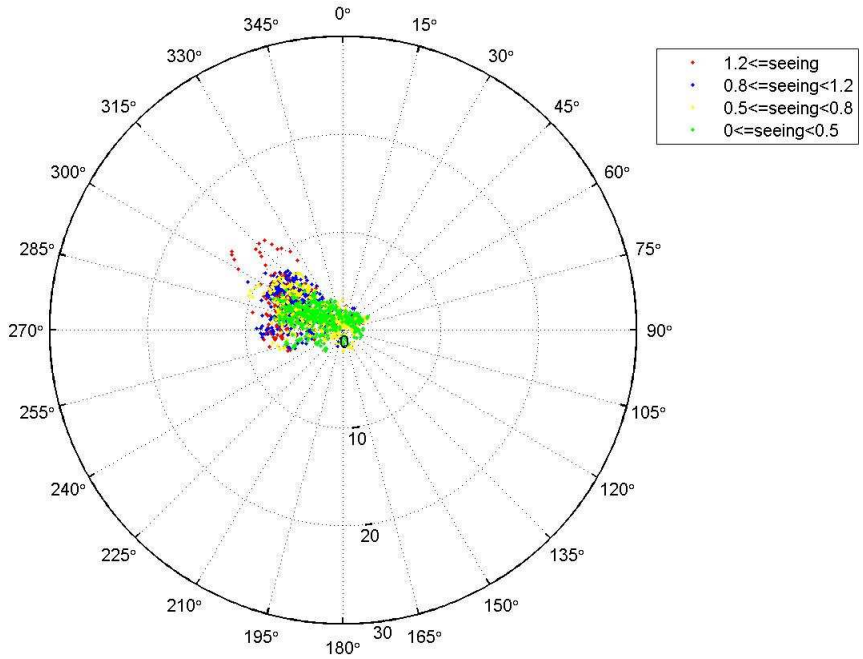

Figure 9.10: A wind compass rose for the E1 cases.

During this time of the year (fall, E1 group) the predominate wind direction is from northwest (NW) which is different from other seasons (E2 and E3 group, Table 5.1), consistent with episodes of *good* seeing, it has a NW direction.

For the E2 cases, it can be noted that *default* and *bad* seeing is when the wind has a southwest – south component (SW – S; 225° to 180°) with an intensity over 8 ms^{-1}. Good seeing is noted with the wind comes from the northwest (NW) with intensities between 0 a 8 ms^{-1}approximately (Figure 9.11).

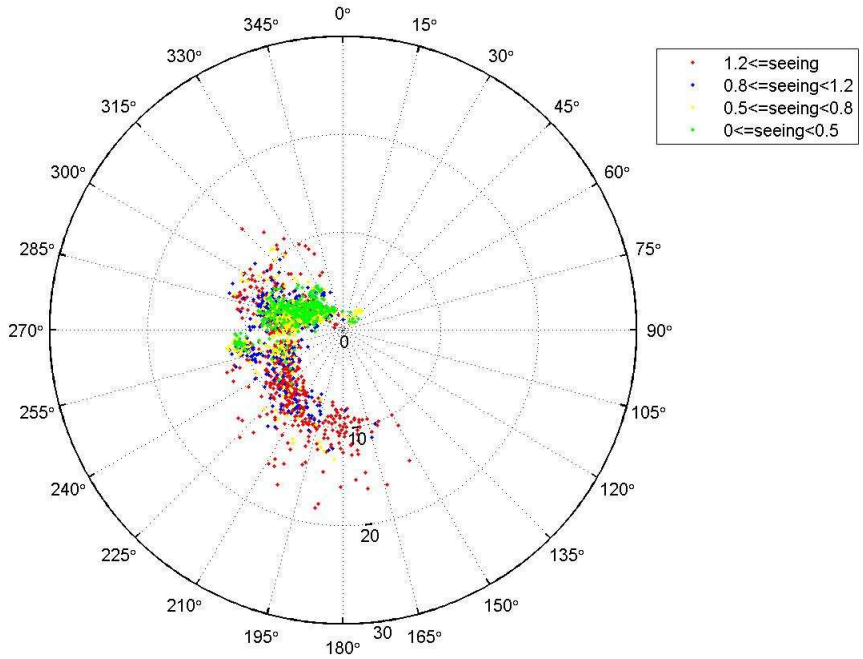

Figure 9.11: Wind and seeing compass rose for E2 cases.

In the E3 period the *default* and *bad* seeing have a wind direction between 240° to 120° (SW – S – SE) approximately with speed over 8 ms^{-1}. For *good* and *very good* seeing it has a direction of 270° to 0° with speed lower than 6 ms^{-1} approximately (Figure 9.12).

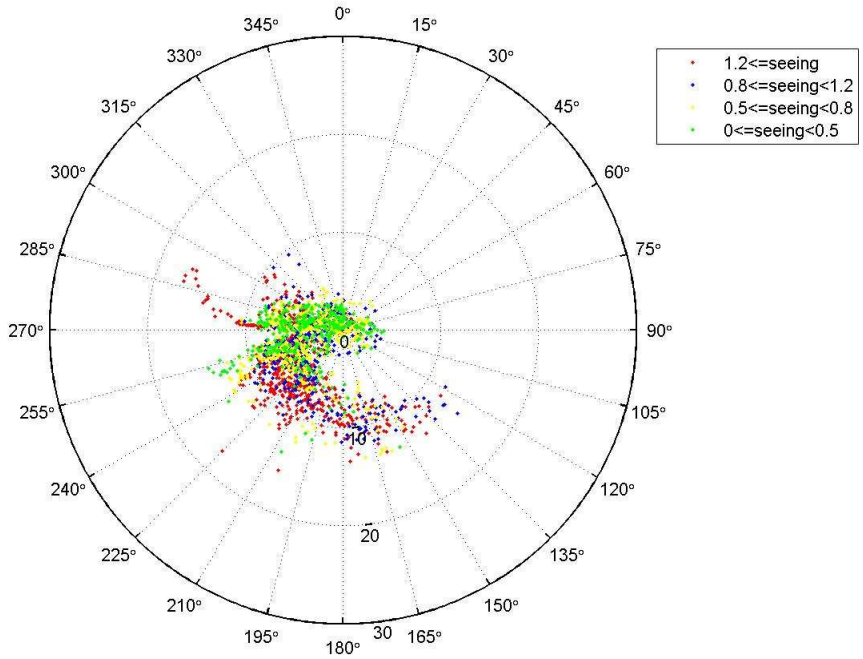

Figure 9.12: Wind and seeing compass rose for E3 cases.

A seasonally analyzis, showed that bad seeing related the wind direction has a rotation from west (W) for the E1 cases until contribution from the southeast (SE) in the E3 case. From this we see the influence of the time of year for the wind direction and speed related to bad seeing. For the case of good seeing the low wind intensities (less than 8 ms^{-1}) and the direction from the northwest (NW) are predominant.

Figure 9.13 shows that there exist a relationship between wind speed averaged every 10 minutes and seeing averaged every 10 minutes in Macón. In this relationship we can see wind speed up to 35 ms^{-1}. From the figure we can distinguish between 0 and 10 ms^{-1} and there is not a clear correlation since the data is dispersed. Between 10 and 18 ms^{-1} appox., a zone with lineal tendencies between seeing and wind intensity can be distinguish. The data is very well related linearly. For the case between 18 to 35 ms^{-1}, the correlation between the data represents a linear tendency, although less than the 10 to 18 ms^{-1} range.

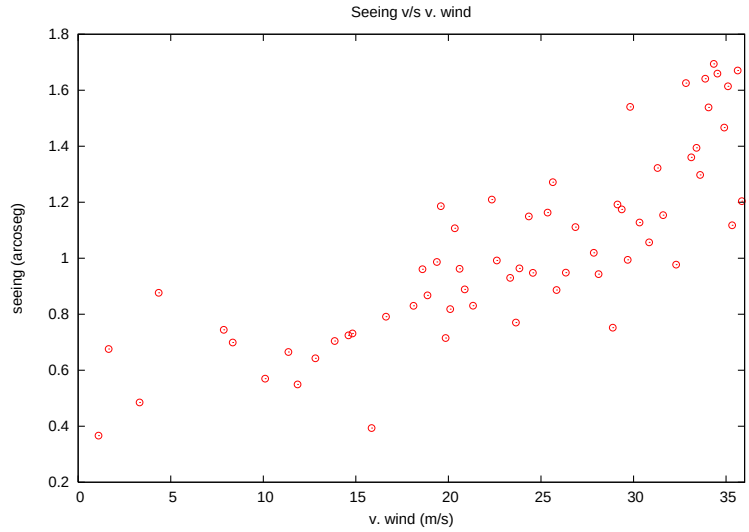

Figure 9.13: Comparison between seeing and wind intensity for the meteorological station at Macón.

9.4 TKE and the Richardson number (Ri)

The TKE (Turbulent Kinetic Energy) and Richardson indices were calculated and compared with the seeing meassured at Tolar and at Macón (Chapter 8). In the first approximation both the TKE and Richarson showed that the greatest amount of turbulence is found at the lower layers near the surface (Figure 9.14 and 9.15). This compared with seeing and the turbulence measured at Tolar with the MASS instrument might be a good indicator for good and bad seeing.

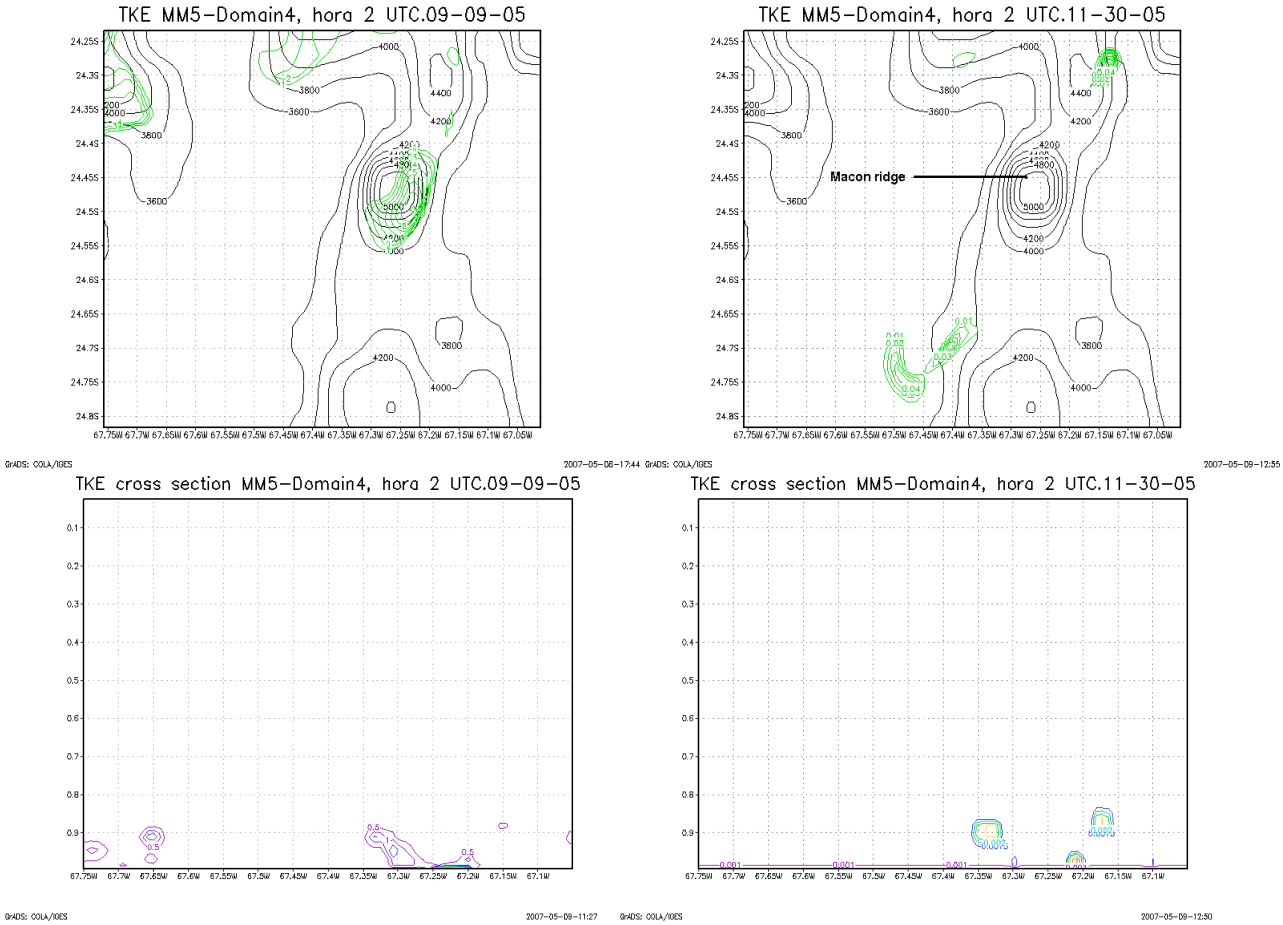

Figure 9.14: Comparison between TKE for a bad and good case of seeing. On the above line, a horizontal cut of domain 4; the bottom line shows a vertical cut above the Macón latitude.

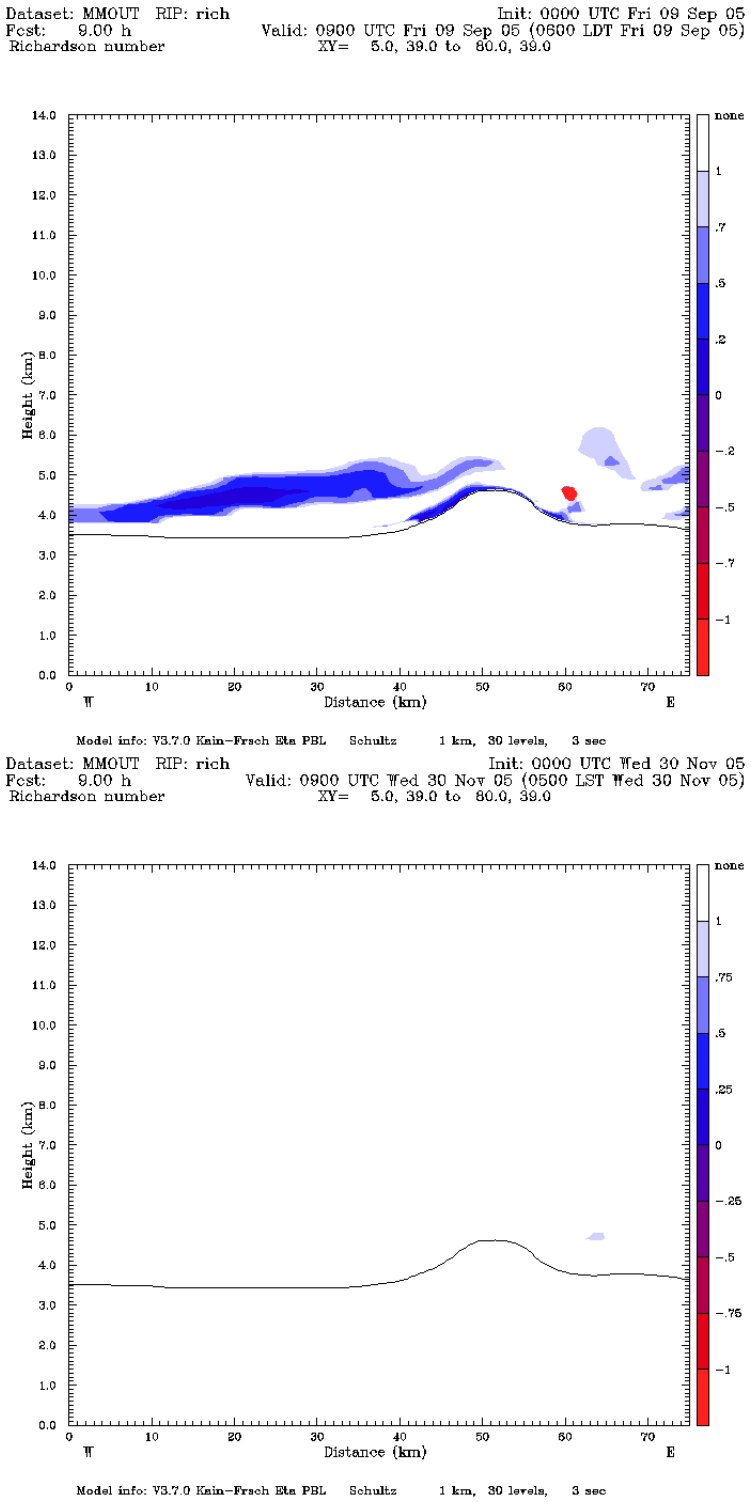

Figure 9.15: Richardson number for a bad case (above) and a good case (below) of seeing.

Later, the column total for the simulated TKE by the MM5 model was compared with seeing calculated for Macón (Chapter 8). To do this the TKE values entered for the model at the 30 levels of altitude at coordinates sigma were added, thus there was an attempt to relate these two variable. Figure 9.16 shows that the TKE values have a base close to value 6 with les variability than seeing. This figure shows that thee does not exist a clear relationship between the data.

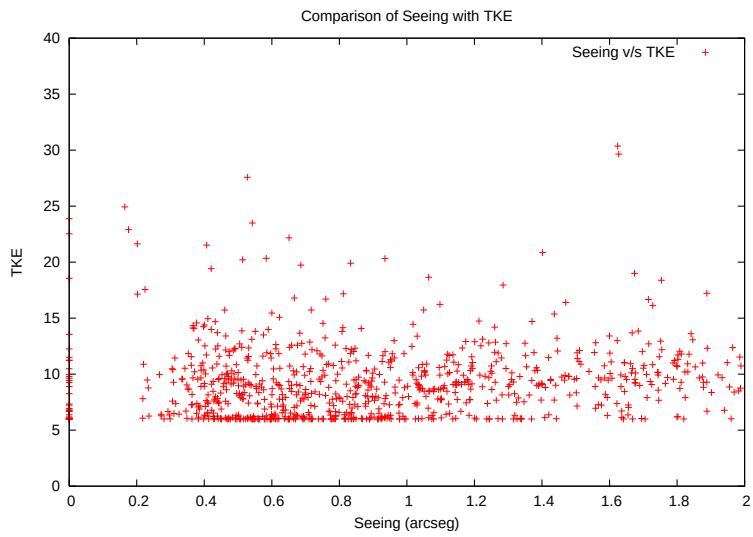

Figure 9.16: Comparison between TKE and seeing for Macón.

Also, an analysis of turbulence data (C_n^2) registered for MASS at different levels was done. Figure 9.17 shows the TKE compared at 2,4, and 8 Km from the altitude above Macón. The variability that TKE has is very low, almost nil at all levels. This is mainly due to the fact that MM5 estimates the turbulence (TKE) close to the surface; towards higher altitudes this has a constant value of 0.2. It should be mentioned that the parameterization used to calculate TKE with MM5 (section 4.4) was only one of the three that exist for this purpose. Due to technical reasons of compilation we could manage to use only this option. In a future study we will evaluate the other two options of parameterization of TKE of the MM5 modeling system.

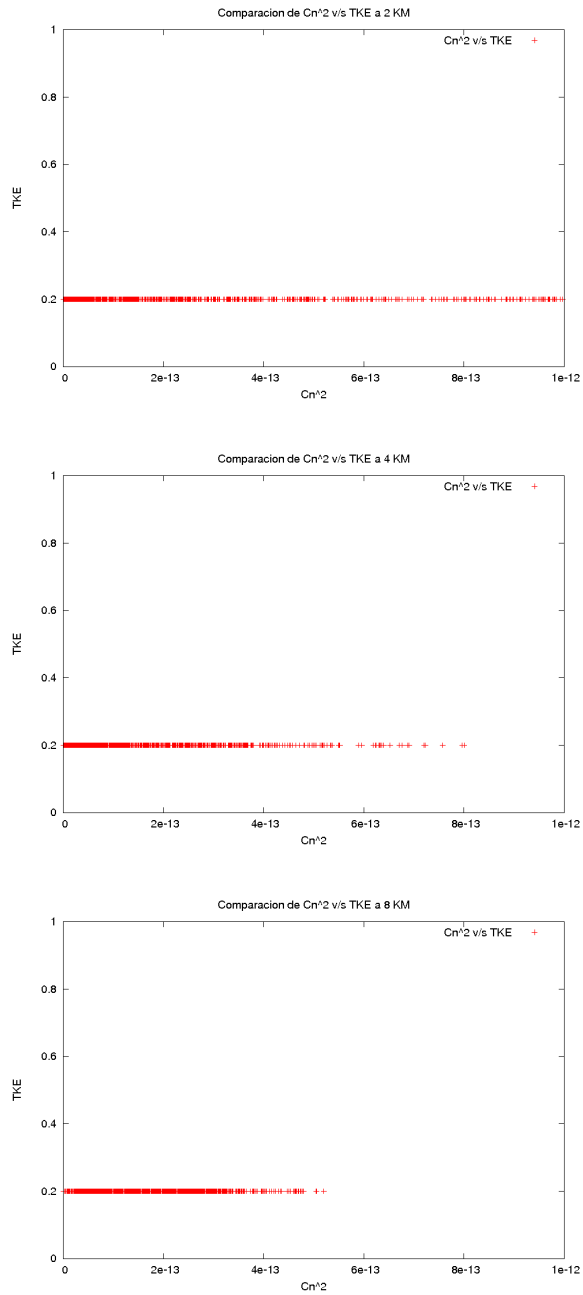

Figure 9.17: TKE compared with C_n^2 at 2, 4 and 8 km above Macón

For the Richardson number (Ri) case, two calculation methods were used: one made by the RIP

program as part of the suite of the MM5 modeling system, which yields vertical graphs as in Figure 9.15. The second way of calculating was with the data from the model using the following relationship:

$$Ri = \frac{g}{T}(\frac{\nabla T_p}{\nabla V^2})$$

where g is gravity,, T is the layer temperature referent; ∇T_p is the potencial temperture gradient in one layer, and ∇V^2 is the wind module gradient in a layer using this relationship. With this last formula we compare the Ri versus the Seeing. Figure 9.18 shows this relationship where Ri has a concentration very close to 0 (zero) and values very scattered. There is no relationship between the data of the variables, which is due to the fact that Ri stays at a cosntant value of 0 when the seeing varies.

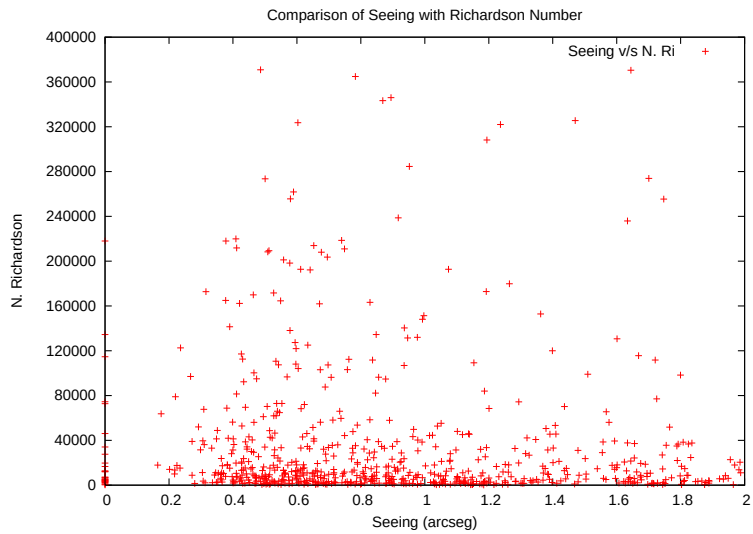

Figure 9.18: Comparison of the Richardson number with seeing in Macón.

In addition, a comparison between Ri and turbulence data (C_n^2) from the MASS instrument at 2, 4 and 8 km above Macón was conducted. Figure 9.19 shows that the values fo Ri at 2 km is concentrated below 60 (adimensional), with small variability. For the 4 km case, the vaules are very similar to those at 2 km, concentrated below 60 (adimensional) of the Ri. For the 8 km case at 8, the variability is concentrated at these values and they are not corelated. As with the previous case, the values of Ri at altitudes do not show a relationship with the turbulence measured by MASS.

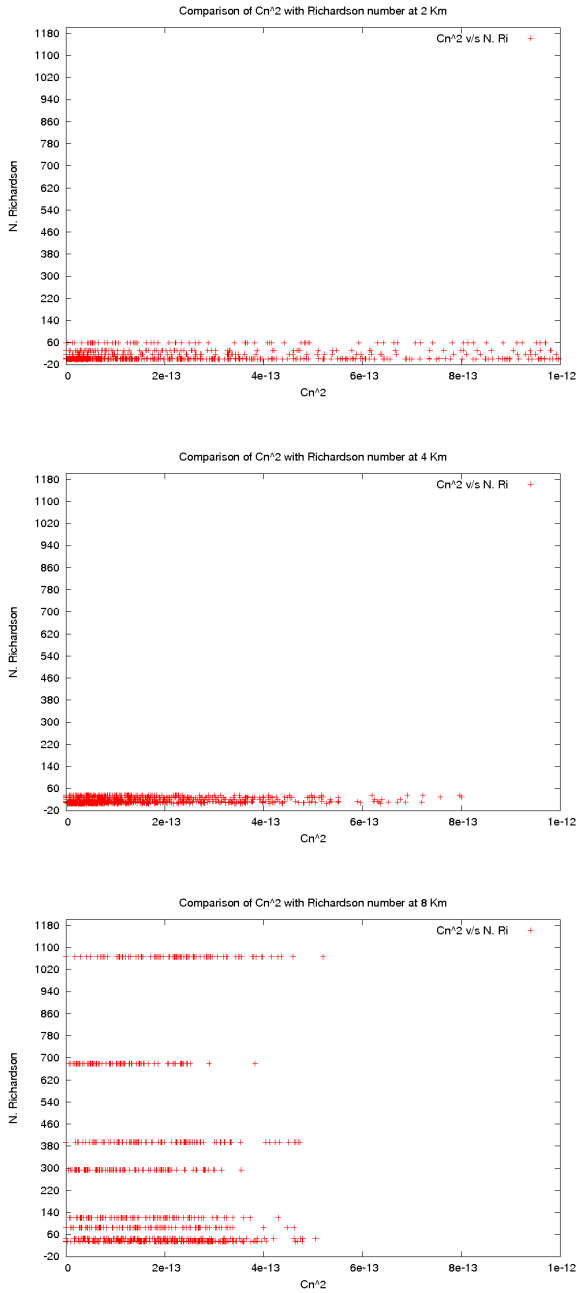

Figure 9.19: Comparison of Ri with turbulence data (C_n^2) at 2, 4 and 8 km above Macón.

The comparison of these indices (TKE and Ri) with the real data (seeing and turbulence(C_n^2))

show a good approximation with the turbulence that occurs at lover levels close to the surface. But, at higher altitudes the values are constant. The small variability indicates that as an estimation tool from turbulence at high levels, it is not optimal.

Chapter 10

Conclusions

The Macón area, site pre-selected for the construction of the ELT (Extremely Large Telescope), is considered one of the optimal zones for astronomy development and the activity that this aids in. At this site, during 2005, a total of 126 measured nights of atmospheric turbulence (C_n^2) and seeing by the MASS instrument were registered, also measurements of standard meteorological variables from a weather station that was located at the summit of Macón (4,600 m.a.s.l.). These measurements served as a basis for this study to analyze and compare the meteorology conditions of Macón and its relationship to the seeing. The use of meteorological information from numerical models was fundamental to this study. This in fact is how the MM5 modeling system has beeing used to analyze the local meteorology conditions of the Macón zone.

10.1 Local meteorology

Macón is surrounded by mountains, on the west by the Andes Mountains and on the east by more mountain chains. The complex orography has made it a fundamental factor for analyzing the local meteorology of this zone Climatologically, there is a marked pattern of circulation from the west predominance of semipermanent and not very humid subtropical anticyclones from the south pacific, which are altered by synoptic situation like HV and JS, which have a duration of time less than the synoptic patterns of PA or BT. The synoptic analysis for the cases studied confirm this situation, where the major instability contribution are the HT, which can last a day. The HT are present all over the year. Its seasonal analysis for fall, winter, and spring (E1, E2, E3) show that the same pattern is present in every period with subsynoptic development time ($\geq$ day). There exists a local meteorological component, controlled by the orography, that makes this place a very notably unstable zone. The airflow is strongly altered by mountain summits forming mountain waves [Whiteman, 2000] that disrupt the atmosphere from the west to Macón, on the surface leading to the salt marsh of Arizaro, a region with an average altitude of 3,500 m.a.s.l. extensive and flat which shows thermal stability close to the surface dominated mainly by the radiation. Here a secondary circulation exist that is formed in the first 500 m approximately over the surface. This secondary circulation does not have a strong vertical component in a way that interacts with higher levels.

The analysis showed that Macón local meteorology is dominated by winds coming from the west, rotating throughout the year toward the southwest from fall to spring. The wind that generally reaches Macón is parallel to its summit (4,600 m.a.s.l) with wind speed that average 6 ms^{-1}. This

was concluded based on the analysis of registered wind by the meteorological station at Macón and the analysis of trajectories from the MM5 model, where in more than 90% of the cases studied, the airflow from levels below the summit of Macón did not reach it.

On the other hand, the airflow that reaches the summit and 1/2km of altitude above Macón do not come, during one night interval, from Paranal. This discard the idea that the turbulence measured at Paranal in low levels can reach the summits of Macón.

10.2 Seeing

Two criteria were considered for the calculation and later analysis of seeing; one above Tolar that the MASS instrument measures and the other for Macón, eliminating the two first levels of measurement of atmospheric turbulence by the MASS instrument (0.5 and 1 km respectively) adequate for estimating the atmospheric thickness from the summit of Macón. This criterion was adopted considering the previous trajectory analysis, where it was shown that the air that reaches Macón and 1/2 km above it, does not influence low levels (salt marsh of Arizaro). The seeing measured in Macón has a median of 0.82" and a superior maximum of 3". The statistical analysis showed that 61.2% of the data with seeing < 1, correspond to 77 days of the total 126, but on 109 days there were entries of seeing $=>$ 1 corresponding to 38% of the data. It was also estimated that the seeing would diminish on average as the night progressed, due to the cooling of the atmosphere close to the surface by radiation and the lower thermal contrast that is produced at these levels. Compared with other atmospheric sites, Macón has a seeing on average almost similar to La Silla, with a median close to 0.8", but with a less cumulative curve.

To analyze the seeing a classification of episodes was done. We adopted the one used in Paranal from adaptive optic. We found that 47% of the nights measured had a value of the median corresponding to a bad night (seeing > 1.2"), this compared with the wind speed, shows that the bad seeing events are present when the wind velocity has a southwest $-$ south $-$ southeast component, which varies seasonally. The bad seeing in fall is concentrated from the southwest in order to arrive in spring with wind direction from the south $-$ southeast with values above the 20 ms^{-1}.

Also, a good relationship with wind speed below 35 ms^{-1} was found. This justifies what was shown by the wind rose, where the bad seeing relates to major intensities of wind speed.

In order to find a relationship between seeing and a meteorological variable, the isotherm of 320 K of potential temperature was analyzed, with the purpose to relate the thermal thickness (vertical distance between isotherms) and the seeing. Unfortunately, no relationship was obtained.

Previous studies showed that the major contribution of seeing is turbulence from levels near the surface. This is in contrast with indices of atmospheric turbulence simulated by the MM5 model. Analysis of TKE was done contrasting the turbulence measured by MASS at different levels of altitude. The correlation found for higher levels (2, 4, and 8 km) were not good, since the TKE index is capable of showing turbulence at levels close to the surface. The analysis using the Richardson number (Ri) also shows that it is sensitive for turbulence produced at low levels, compared with the turbulence at high levels such as 2, 4, and 8 km.

The MM5 modeling system contrasted with the data observed in Macón showed a negative error for temperature and a positive for the wind speed. In order to improve these values, applying the Kalman filter was suggested in order to eliminate systematic errors of the model, also suggested was the integration of simulations with the data observed through the meteorological station. Evaluating the parameterization that TKE calculates in order to implement the one that is the most adequate for this type of complex terrain was also suggested. There are experiences that exist at Mauna Kea

Weather Center, Hawaii, where they simulate using the MM5 the vertical turbulence profile(C_n^2). This can also be implemented in future studies.

In summary, the meteorological conditions and the seeing at Macón have a very conditioned relationship by the complexity of the terrain. There is a very good relationship between measured variable such as wind speed with respect to *good* and *bad* seeing. On the other hand, the MM5 is capable of capturing many details of the conditions on synoptic and local scales, but the indices of turbulence simulated have greater exactitude only at lower levels close to the surface.

Bibliography

[Alvarez, C., 2005] Alvarez, C., 2005: Análisis multivariable en meteorología de contaminación atmosferica para fundición Potrerillos. Tesis para el grado de Licenciatura en Meteorología. Universidad de Valparaíso.

[Ballard et al., 1991] Ballard, S. P., Golding, B. W., Smith, R. N., 1999: Mesoscale model experimental Forescasts of the Haar of Northeast Scotland. *Nom. Wea. Rev.*, 119, 2107-2123.

[Banta et al, 2003] Banta, R., Pichugina, Y., Newsom, R., 2003: Relationship between Low-Level Jet Properties an Turbulence Kinetic Energy in the Nocturnal Stable Boundary Layer. *J. Atmos. Sci. 60,* 2549-2555.

[Cuevas, 2005] Cuevas, O., 2005: Análisis de ozonosondas en Rapanui: Climatología, masas de aire y su impácto en el ozono troposférico. Tesis para el grado de Licenciatura en Meteorología. Universidad de Valparaíso.

[Garreaud, 1999] Garreaud, R., 1999: Multiescale analysis of the sumertime precipitation over of the central Andes. *Mon. Wea. Rev.,* 127, 901-921.

[Grell et al., 1994] Grell, G. A., Dudhia, J. and Stauffer, D. R., 1994: A description of the fifth-generation Penn State/NCAR mesoescale model (MM5). NCAR Technical Note, NCAR/TN-398+SRT, 117 pp.

[Kain and Fritsch, 1993] Kain, J. S., Fritsch, J. M.;1993: Convective parameterization for mesoscale model: the Kain-Fritsch scheme. The representation of cumulus in numerical models; Meteor. Monogr. *Amer. Metor. Soc.*

[Mlawer et al., 1997] Mlawer, E. J., Taubman, S. J., Brown P. D., Iacono, M. J., and Clough S. A., 1997: Radiative transfer for inhomogeneous atmosphere: RRTM, a validated correlated-k model for longwave. *J. Geophys. Res.*, 102 (D14), 16663-16682.

[Ramos, 2003] Ramos, I., 2003: Validación del modelo European Centre for Medium Range Weather Forecasts (ECMWF) para el pronóstico de temperatura en la V Región. Tesis para el grado de Lincenciado en Meteorología. Universidad de Valparaíso.

[Rutlland, J., 1982] Rutlland J., Salinas H., 1982: Frecuencia de ocurrencia de una condición meteorológica desfavorable para la disfusión de contaminantes atmosféricos en al zona central de Chile. *Tralka. Depto. de Geofísica, Universidad de Chile.*

[Sarazin et al., 2002] Sarazin, M., Graham, E., Beniston, M., Riemer, M., 2002: The New Tools for a Global Survey of Potencial Sites for the Future Gigant Telescopes. *SPIE Conf. on astronomical Telescope and Instrumentation, Waikoloa, Hawaii, USA, paper SPIE-4840-54.*

[Schultz, 1995] Schultz, P., 1995: An explicit cloud physics parameterization for operational numerical waether predicction. *Mon. Wea. Rev.,* 123, 3331-3343.

[Shafran et al., 2000] Shafran, P. C., Seaman, N. L., and Gayno, A., 2000: Evaluation of numerical prediction of boundary layer structure during the lake-Michigan Ozone Study. *J. Appl. Meteor.,* 39, 412-426.

[Ulriksen P., 2001a] Ulriksen P., 2001: Meteorología aplicada a contaminación atmosférica. Escuela de postgrado y diplomado en contaminación atmosférica. Facultad de Ciencias Físicas y Matemáticas, Universidad de Chile. Centro Nacional de Medio Ambiente (CENMA).

[Ulriksen P., 2001b] Ulriksen P., 2001: Instructivo para la aplicación de modelos de difusión atmosféricas a efluentes gaseosos. Escuela de postgrado y diplomado en contaminación atmosférica. Facultad de Ciencias Físicas y Matemáticas, Universidad de Chile. Centro Nacional de Medio Ambiente (CENMA).

[White et al., 1999] White, B. G, J. Paegle, W. J. Steenburgh, J. D. Horel, R. T. Swanson, L. K. Cook, D. J. Onton and J. G. Miles, 1999: Short-Term forecast validation of six models. *Wea. Forecast, 14,* 84-108.

[Whiteman, 2000] Whiteman, D. C., 2000: Mountain Meteorology: Fundamentals and applications. *Oxford University Press.*

Internet reference

1. Internet reference 1 : http://www.mmm.ucar.edu/mm5/documents/MM5_tut_Web_notes/MM5/mm5.htm
2. Internet reference 2 : http://www.eso.org/gen-fac/pubs/astroclim/forecast/meteo/verification/LaSilla/index.html
3. Internet reference 3 : http://www.eso.org/gen-fac/pubs/astroclim/paranal/seeing/seewind/
4. Internet reference 4 : http://www.eso.org/gen-fac/pubs/astclim/paranal/asm/mass/MASS-Argentina/MM5/macon_18apr07_eng.pdf

Chapter 11

Appendix

Program for download GFS data daily and automatically

A program written in PERL language that downloads from the ftp of the NCEP the data of the global GFS model, every 6 hours until 72 hours of forecasting is reached. This data corresponds to each day's 00Z.

```
#!/usr/bin/perl
$fecha="gfs.".`date +20%y%m%d00`;
chomp($fecha);
mkdir($fecha);
chdir($fecha);
use Net::FTP;
$ftp = Net::FTP->new("ftpprd.ncep.noaa.gov", Debug => 1);
$ftp->login("anonymous",'-');
$ftp->cwd("/pub/data/nccf/com/gfs/prod/$fecha");
$ftp->get("wafsgfs_P_t00z_intdsk00");
$ftp->get("wafsgfs_P_t00z_intdsk06");
$ftp->get("wafsgfs_P_t00z_intdsk12");
$ftp->get("wafsgfs_P_t00z_intdsk18");
$ftp->get("wafsgfs_P_t00z_intdsk24");
$ftp->get("wafsgfs_P_t00z_intdsk30");
$ftp->get("wafsgfs_P_t00z_intdsk36");
$ftp->get("wafsgfs_P_t00z_intdsk42");
$ftp->get("wafsgfs_P_t00z_intdsk48");
$ftp->get("wafsgfs_P_t00z_intdsk60");
$ftp->get("wafsgfs_P_t00z_intdsk72");
$ftp->quit;
```